Design of Fillet and PJP Welds in CHS-to-CHS Moment T-Connections: Finite Element Investigation

by

Chengcheng Zhang
B.Eng, Beihang University, 2023

A Thesis Submitted in Partial Fulfillment of the
Requirements for the Degree of

MASTER OF APPLIED SCIENCE

in the Department of Civil Engineering

Design of Fillet and PJP Welds in CHS-to-CHS Moment T-Connections: Finite Element Investigation

By

Chengcheng Zhang

B.Eng, Beihang University, 2023

Supervisory Committee

Dr. Min Sun, Supervisor

Department of Civil Engineering

Dr. Cheng Lin, Department Member

Department of Civil Engineering

Abstract

This thesis presents a study to evaluate the effective geometric property approach in AISC 360-22 for design of welds in circular hollow section (CHS)-to-CHS moment T-connections under in-plane bending. Experimental data from previous full-sized connection tests is used to verify a finite element (FE) modelling approach for weld-critical connections. A subsequent FE parametric study, including 137 fillet and partial-joint-penetration groove welded CHS-to-CHS connection models, is performed to cover wide ranges of nondimensional design parameters: branch-to-chord diameter ratio (0.4 to 1.0), branch-to-chord thickness ratio (0.2 to 1.0), and chord slenderness ratio (10 to 50). New formulae in recent research for calculation of the weld effective elastic section modulus for in-plane bending are evaluated, and modifications are proposed. The proposed modifications provide more accurate predictions of weld strength yet still achieve sufficient safety margins.

Table of contents

List of Tables

List of Figures

Acknowledgement

First, I would like to thank my supervisor, Dr. Min Sun, for the continuous and indispensable guidance and instructions. I would also like to thank Dr. Kyle Tousignant and Mr. Zhiyuan Yang from Dalhousie University, for their necessary supporting for this research. And I would like to thank to the friends in Victoria who have helped me in this stage of life. Finally, I would like to thank my family and my wife in the future, Ms. Lu Zhang, for their help and encouragement for my study. I appreciate everyone.

This research was funded by the Natural Sciences and Engineering and Research Council of Canada (NSERC).

Chapter 1: Introduction

For design of welds in hollow structural section (HSS) connections, existing standards and guidelines (AISC 2022; AWS 2020; CSA 2019a; ISO 2013; Packer et al. 2010) acknowledge two approaches:

(i) a "prequalifying approach" where welds are sized to give a resistance that is not less than the branch member yield strength; and

(ii) a "fit-for-purpose approach" where welds are sized to resist the actual force(s) in the connecting branch member.

Connections designed using the first approach will not be weld-critical. This approach is appropriate when there is uncertainty in member forces or when plastic stress redistribution is needed but can often lead to oversized weld. The effective length approach is also known as the fit-for-purpose approach since it produces smaller weld sizes which will lead to less fabrication effort (and lower cost). This approach is particularly useful when the branch member force is low compared to the branch member yield strength, which is often the case in the design of tubular steel truss and girder web members.

AISC 360-22 Section K5 and Table K5.1 (AISC 2022) include equations for the "fit-for-purpose" design of welds in rectangular hollow section (RHS)-to-RHS connections of different types (T-, Y-, X-, overlapped K- and gapped K-) under different loading conditions (branch axial force, branch in-plane and out-of-plane bending). These equations are supported by evidence from a substantial amount of previous research (Frater and Packer 1992a, 1992b; McFadden et al. 2013; Packer and Cassidy 1995; Packer and Sun 2011; Packer et al. 2016; Tousignant and Packer 2015; Tousignant and Packer 2017b; Yaghoubshahi et el. 2019; Tousignant and Packer 2020b).

Relevant experimental and numerical research has been performed by Packer et al. (2016) and Tousignant and Packer (2017a, 2017b, 2018, 2019a, 2019b, 2020a, 2020b), based on which weld design rules for CHS-to-CHS T-, Y- and X-connections under branch axial force have been developed and now, adopted in a Table K5.2 of AISC 360-22.

As a continuation of this effort, Yang and Tousignant (2022) performed experiments on weld-critical CHS-to-CHS moment T-connections with fillet and partial-joint-penetration (PJP) groove welds. A total of 11 connection tests was performed to examine the uneven stress distribution around the welded joints, and an effort was made to develop a formula for calculation of the weld effective elastic section modulus based on the available experimental data.

In this research, Yang and Tousignant's (2022) connection test results are used to verify a finite element (FE) modelling approach for weld-critical CHS-to-CHS moment T-connections. A subsequent FE parametric study, including 137 fillet and partial-joint-penetration groove welded CHS-to-CHS connection models, is performed to cover wide ranges of nondimensional design parameters with branch-to-chord diameter ratios (β) ranging from 0.4 to 1.0, branch-to-chord thickness ratios (τ) ranging from 0.2 to 1.0, and chord slenderness ratio (2γ) ranging from 10 to 50. A new approach to calculate the weld effective elastic section modulus is developed, and a first-order reliability method (FORM) analysis is performed to examine its accuracy.

Chapter 2: Literature Review

For design of welds in RHS-to-RHS connections, AISC 360-22 Section K5 (AISC 2022) considers the uneven load transfer along the line of weld. The nominal strength of the welded joint under axial loading (P_n) and under in-plane and out-of-plane bending ($M_{n\text{-}ip}$ and $M_{n\text{-}op}$) are given as:

$$P_n = F_{nw} t_w l_e \quad (1)$$

$$M_{n-ip} = F_{nw} S_{ip} \quad (2)$$

$$M_{n-op} = F_{nw} S_{op} \quad (3)$$

where l_e = weld effective length; t_w = weld throat size; S_{ip} and S_{op} = weld effective elastic section modulus for in-plane bending and out-of-plane bending moment, respectively. To calculate the design strength of the weld, a resistance factor of ϕ = 0.75 and 0.80 is multiplied by Eqs. (1) – (3) for fillet weld and PJP groove weld respectively, according to the LRFD method of AISC 360-22 Chapter J. F_{nw} is the nominal strength of the weld metal in accordance with Chapter J, which can be calculated using Eqs. (4) and (5).

$$F_{nw} = 0.60 F_{EXX} (1.0 + 0.50\, sin^{1.5}\, \theta) \text{ for fillet welds} \quad (4)$$

$$F_{nw} = 0.60 F_{EXX} \text{ for PJP groove welds} \quad (5)$$

where $(1.0 + 0.50 sin^{1.5}\theta)$ is a directional strength-increase factor for fillet welds and θ is the angle between the line of application of the branch force and the weld longitudinal axis (in degrees). AISC 360-22 specifies that for welds of plates and branches to RHS, the directional strength-increase factor shall not be used in the strength calculation. On the other hand, recent research (Tousignant and Packer 2019b) has shown that the directional strength-increase factor is appropriate for design of welds in CHS-to-CHS connections. The angle θ is however difficult to

determine directly for CHS-to-CHS connections due to the complex weld shape at the branch-to-chord intersection. Recent research by Tousignant and Packer (2019b) has shown that it is reasonable to simply use the angle between the branch and chord members (θ_b) for weld strength calculations when $60° \leq \theta_b \leq 90°$.

For CHS-to-CHS T-, Y- and X-connections under branch axial force, previous research by Tousignant and Packer (2018) showed that the effective-to-total weld ratio (l_e/l_w) is largely influenced by the parameters β and 2γ (= D/t). The branch-to-chord member angle (θ_b) had only minor effect. Based on the experimental and numerical data on weld-critical connections ($60° \leq \theta_b \leq 90°$, $10 \leq D/t \leq 50$, $0.1 \leq \beta \leq 0.5$, and $0.2 \leq \tau \leq 1.0$), it was proposed that l_e can be calculated using Eqs. (6) and (7) for axially loaded CHS-to-CHS connections within the ranges of nondimensional parameters covered by the research. This approach has already been adopted in the AISC 360-22 Table K5.2 (AISC 2022). It should be noted that this approach approximates l_w by considering "branch-angle distortion" (i.e., the transformation of a circular weld into an ellipse caused by a change in θ_b) but ignoring "beta-ratio distortion" (which causes the plane of the elliptical weld to further distort into a saddle shape). Therefore, the estimated weld effective length is expected to be conservative for connections with higher β-ratios than those covered in the study.

$$l_e = \frac{4}{\sqrt{2\beta(D/t)}} l_w \leq l_w \tag{6}$$

$$l_w = \pi D_b \frac{1 + 1/\sin\theta}{2} \tag{7}$$

To develop recommendation for calculations of weld effective elastic section moduli for CHS-to-CHS T-connections under in-plane bending, Yang and Tousignant (2022) carried out 11 full-sized weld-critical T-connection tests ($0.31 \leq \beta \leq 0.91$, $31 \leq D/t \leq 46$, $0.70 \leq \tau \leq 1.00$, $\theta_b = 90°$). Connections with $\beta < 0.47$ were fillet-welded and connections with $\beta \geq 0.47$ were PJP-welded with

the local dihedral angles (Ψ) between 60° and 120° around the perimeter of the welded joints. The test set-up and connection nomenclature are shown in Fig. 2.1.

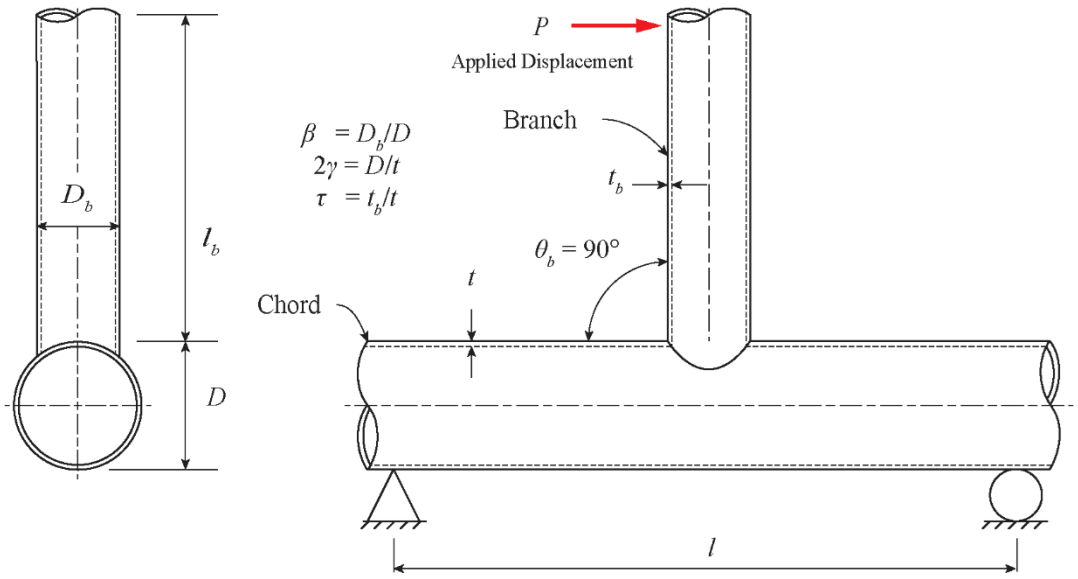

Fig. 2.1. CHS-to-CHS moment T-connection test configuration for in-plane bending and nomenclature

Based on the available data, and the recommendations in AWS D1.1 (AWS 2015), Yang and Tousignant (2022) proposed a preliminary formula for calculation of S_{ip} (Eq. (8)). Detailed discussion of the formula can be found in Yang and Tousignant (2022) but, in general, Eq. (8) simplifies the complex three-dimensional saddle shape of the welded joint into a two-dimensional oval shape. It considers the branch-angle distortion but ignores beta-ratio distortion (similar to Eq. (7)).

$$S_{ip} = t_w \frac{(3 + 1/\sin\theta)}{4\sin\theta} \pi \left(\frac{D_b}{2}\right)^2 \tag{8}$$

The above experimental research is particularly useful as it shed light on the behaviour of welded joints in CHS-to-CHS moment T-connections. Using Eqs. (2), (4), (5) and (8), the

predicted weld joint strengths were calculated for the 11 connection specimens tested. The comparison between the limited amount of test data and the corresponding predicted strengths produced an average actual-to-predicted ratio of 1.61 and coefficient of variation (COV) of 0.15, which shows that the proposed preliminary approach can in some cases be quite conservative. Considering the complex weld shape and stress status in such connections, further research is needed to supplement the experimental investigation performed by Yang and Tousignant (2022) (which consisted of four fillet-welded specimens and seven PJP-welded specimens). Specifically, more data is needed to further examine the behaviours of the two different weld types.

In light of this, the research presented herein comprises a comprehensive FE parametric study including a total of 137 weld-critical fillet and partial-joint-penetration groove welded CHS-to-CHS connection models that cover wide ranges of nondimensional design parameters.

Chapter 3: FE Modelling Approach and Verification

3.1 General

To validate the accuracy of the FE modelling approach applied in this research, 11 CHS-to-CHS T-connection models were developed to replicate the experiments performed by Yang and Tousignant (2022) with the same dimensions, material properties as well as boundary and loading conditions. The connection dimensions and key connection test results are summarized in Table 3.1. The connection specimen IDs in the table include 4 components: the first component, "T", indicates the connection configuration; the second component is the nominal chord diameter; the third component is the nominal branch diameter; and the last component, "F" or "P", indicates whether the joint is fillet- or PJP-welded.

Research by Luvites and Post (1988) has shown that the branch-to-chord diameter ratio (β) must not exceed 0.5 for 90° CHS-to-CHS T-connections if fillet welds are to be used with the local dihedral angle (angle between base metal fusion faces) < 120°. Hence, Yang and Tousignant (2022) adopted this recommendation in their experimental research (i.e., all fillet-welded connections have $\beta \leq 0.5$ and all PJP-welded connections with $\beta > 0.5$). For PJP welds, the local dihedral angle is less important since the chord can be bevelled to allow sound penetration to the root.

In this research, the FE modelling was performed using ANSYS (ANSYS 2021). For all connection models, the boundary conditions at the two chord ends simulated the actual test setup where a pin support and a roller support were applied. The connection tests reported by Yang and Tousignant (2022) were displacement controlled. Similarly, in this research, a horizontal displacement was applied to the branch to generate the branch in-plane bending. The horizontal

forces at different horizontal displacement levels were determined by ANSYS. For calculation of the magnitude of the branch in-plane bending moment, the branch length (l_b), which is the distance between the line of application of the horizontal displacement and the crown of the welded joint, was multiplied by the horizontal force. All branch lengths (l_b) used in the FE analysis were the same as those in the experimental tests.

Table 3.1. Connection dimensions and comparison of experimental and FE results.

Specimen ID	Branch	Chord	t_w	M_a[1]	M_{FE}[3]	Δ_a[2]	Δ_{FE}[3]	M_a/M_{FE}	Δ_a/Δ_{FE}
	$D_b \times t_w$ (mm)	$D \times t$ (mm)	mm	kN-m	kN-m	%	%		
T324-127-1F	127.6 × 8.9	325.0 × 9.3	2.96	36.47	29.97	1.13	0.70	1.22	1.62
T356-127-1F	127.6 × 8.9	355.9 × 9.3	2.32	28.33	25.52	0.54	0.51	1.11	1.06
T406-127-1F	127.6 × 8.9	407.4 × 8.9	2.81	28.74	26.75	0.98	1.08	1.08	0.91
T406-127-0.7F	127.6 × 8.9	407.4 × 11.8	2.24	31.59	26.05	0.49	0.30	1.21	1.62
T273-127-1P	127.6 × 8.9	274.0 × 8.9	4.58	39.77	37.80	3.08	3.12	1.05	0.99
T356-273-1P	274.0 × 8.9	355.9 × 9.3	5.57	155.88	155.70	3.19	3.25	1.00	0.98
T356-324-1P	325.0 × 9.3	355.9 × 9.3	5.03	199.83	217.40	1.55	2.19	0.92	0.71
T406-273-1P	274.0 × 8.9	407.4 × 8.9	4.42	129.97	127.73	2.57	2.47	1.02	1.04
T406-324-1P	325.0 × 9.3	407.4 × 8.9	4.11	188.97	176.27	3.21	1.87	1.07	1.71
T406-273-0.7P	274.0 × 8.9	407.4 × 11.8	4.95	144.97	169.87	0.99	2.35	0.85	0.42
T406-324-0.7P	325.0 × 9.3	407.4 × 11.8	5.36	251.60	241.86	2.64	2.38	1.04	1.11

[1] Actual (experimental) weld fracture in-plane moment.
[2] Actual (experimental) chord indentation at weld fracture (as % of measured chord diameter).
[3] M_{FE} and Δ_{FE} are FE values corresponding to M_a and Δ_a.

To reduce computational effort, for each of the 11 FE verification models only one half of each connection was modelled considering the symmetry of geometry, boundary and loading conditions. Typical FE models of fillet- and PJP-welded connections are shown in Figs. 3.1 and 3.2, respectively. At the “cut face”, a “symmetry boundary condition” was applied. A sensitivity analysis was applied to ensure that the meshing was carried out appropriately and that all models were not excessively large (computationally), but still provided convergence. To ensure that the load transfer from the branch to the chord was only through the weld, at the initial stage a gap of

0.25 mm was modelled between the two members at the joint location (for both fillet- and PJP-welded connections). The 0.25 mm value was recommended by Tousignant and Packer (2018) in modelling weld-critical CHS-to-CHS X-connections. All FE models were developed to consider material nonlinearity and geometric nonlinearity (large deformation). The analyses were performed with time-step displacement control using the full Newton-Raphson method.

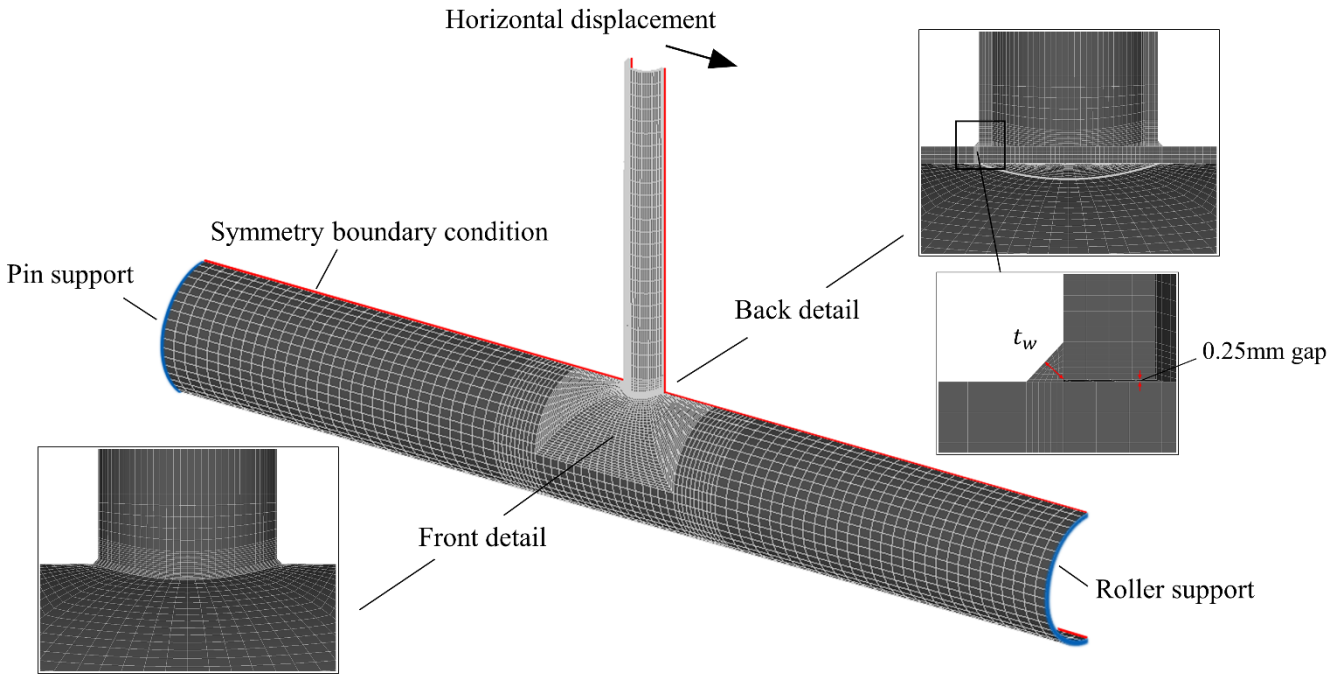

Fig. 3.1. FE details of T406-127-0.7F (Fillet weld)

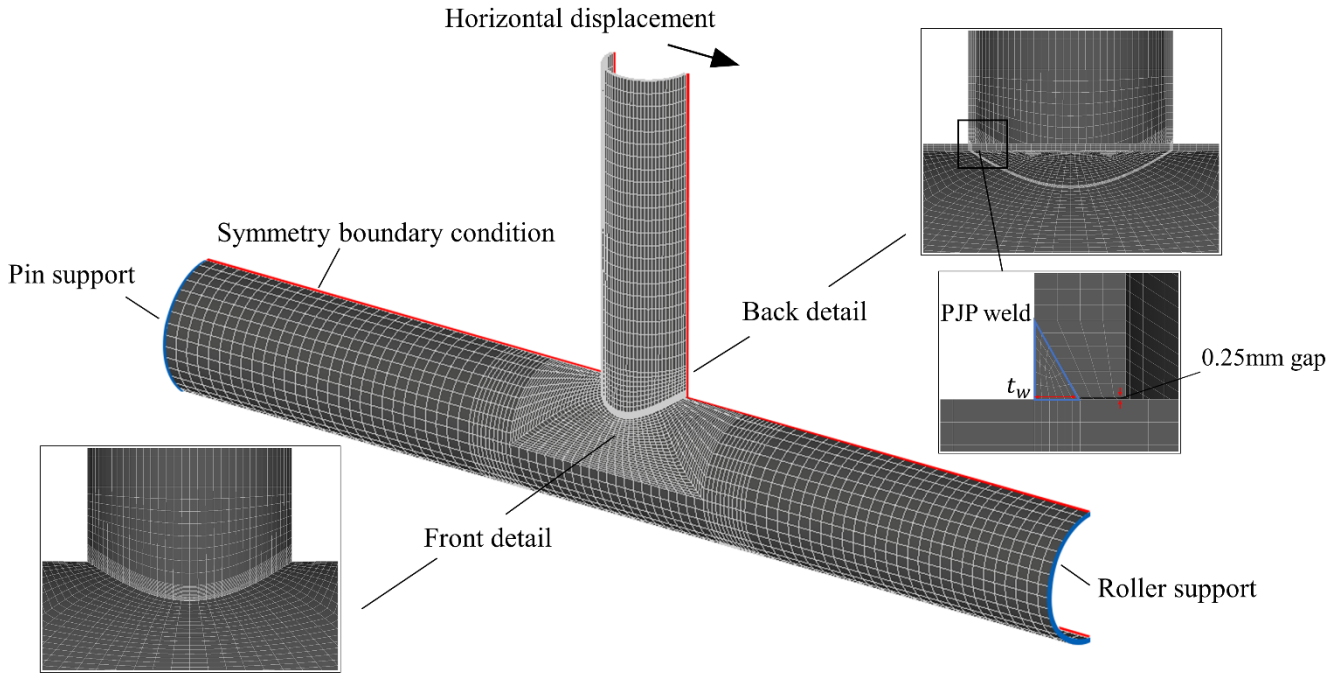

Fig. 3.2. FE details of T406-273-1P (PJP weld)

3.2 Material Properties

In the experimental program reported by Yang and Tousignant (2022), tensile coupon tests were performed to determine the material properties of the CHS and the as-laid weld materials of the 11 connection specimens in Table 3.1. When replicating the 11 connection specimens in ANSYS (ANSYS 2021), the experimentally obtained engineering stress-strain relationships of the CHS and weld materials were converted to true stress-strain relationships for the nonlinear FE analyses.

Specifically, prior to necking the engineering stress (σ)- and strain (ε)- values are converted to the true stress (σ_T) and strain (ε_T)-values by Eqs. (9) and (10):

$$\sigma_T = \sigma(1 + \varepsilon) \tag{9}$$

$$\varepsilon_T = ln(1 + \varepsilon) \tag{10}$$

After necking, the true strain (ε_T)-values are still obtained by Eq. (10), while true stress (σ_T)-values are calculated using an iterative method proposed by Ling (1996), which uses a weighting factor to approximate the true stresses between an upper bound and a lower bound:

$$\sigma_T = \sigma_T' \left[w(1 + \varepsilon_T - \varepsilon_T') + (1 - w) \left(\frac{\varepsilon_T{}^{\varepsilon_T'}}{\varepsilon_T'{}^{\varepsilon_T'}} \right) \right] \tag{11}$$

where σ_T' = true stress at onset of necking (ultimate strength); ε_T' = true strain at onset of necking; w = weighting factor.

The weighting factors in Eq. (11) for the six CHS (Table 3.1) and the as-laid weld materials were determined using the approach recommended by Tousignant and Packer (2018) and Yahoubshahi et al. (2019) (wherein the detailed steps can be found). In summary, seven FE tensile coupon models (six for the six CHS and one for the as-laid weld material) were developed and analysed to replicate the experimentally tested tensile coupons. The weighting factors were determined by matching the FE stress-strain curves with the tensile coupon test results. The FE stress-strain relationships were then used in the subsequent connection modelling. Typical comparisons of the engineering and true stress-strain relationships from the experimental testing and numerical simulation are shown in Fig. 3.3 for the CHS and as-laid weld materials where good agreements can be seen. It should be noted that this research studies weld-critical connections since the objective is to develop weld design recommendations for CHS-to-CHS moment T-connections under in-plane bending. The FE curves for the as-laid weld material in Fig. 3.3 at this stage do not show the fracture point. The development of the fracture criteria for use in the subsequent FE simulation of connections is discussed in Section 3.4.

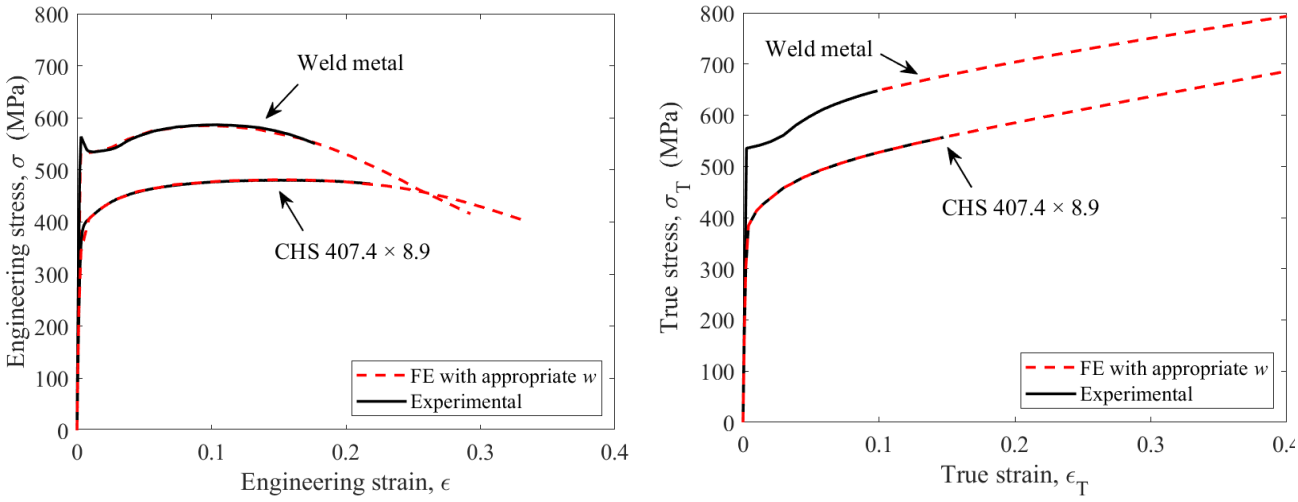

(a) Engineering stress-strain curve (b) True stress-strain curve

Fig. 3.3. Comparison of typical FE and experimental stress-strain relationship

3.3 Connection Modelling Details

For both fillet-welded and PJP-welded connection models, using the approach in Yang and Tousignant (2022) the applied moment-versus-chord deformation curves were obtained. The effects of various FE modelling details on the applied moment-versus-chord deformation curves were examined using a sensitivity analysis. Eight-noded solid brick element SOLID 185 in ANSYS (ANSYS 2021) were used, with uniform reduced integration with hourglass control factor of 1.0, to model the branch, chord and weld area. As shown in Fig. 3.4, four layers of solid elements were applied through the branch and chord wall thicknesses. For connection models with small branch-to-chord diameter ratios ($\beta < 0.60$), the circumference of the branch was divided into 80 elements (40 elements for one half of the FE model). For connection models with small branch-to-chord diameter ratios ($\beta \geq 0.60$), the circumference of the branch was divided into 120 elements (60 elements for one half of the FE model) and the weld legs were meshed with seven elements. As shown in Fig. 3.4, the welded joint and nearby locations are finely meshed in a reasonable manner to obtain an accurate simulation of the uneven load transfer through weld. The mesh

became gradually coarser along the branch and chord members as the distance from welded joint increases.

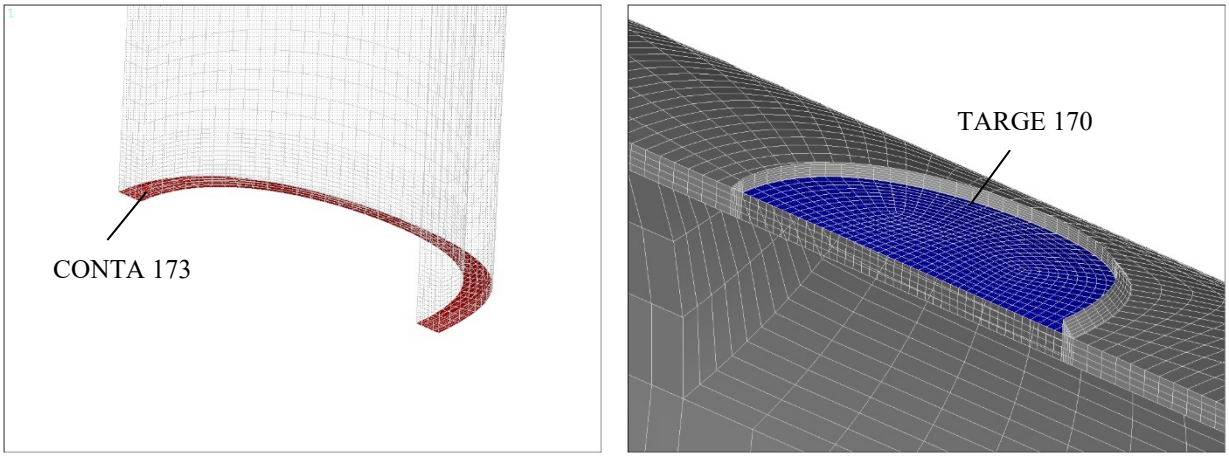

(a) Branch connecting face (b) Chord connecting face

Fig. 3.4. Connection mesh patterns and contact element details

As discussed in Section 3.1, to ensure that the load transfer from the branch to the chord was only through the weld at the initial loading stage, a gap of 0.25 mm, recommended by Tousignant and Packer (2018), was modelled between the two members at the joint location, for both fillet- and PJP-welded connections. On the other hand, previous research on the behaviour of welded joints in RHS-to-RHS moment T-connections revealed a bearing mechanism on the compressive side of the chord connecting face as the applied moment increases (Yaghoubshahi et al. 2019). In this research, to properly simulate the bearing mechanism and to prevent incorrect penetration of branch elements into chord elements, the contact element details at the branch and chord connecting faces were carefully defined (Fig. 3.4). Specifically, CONTA173 elements were used to simulate contact and sliding between three-dimensional target surfaces and a deformable surface defined by these elements. TARGE170 were used to simulate various three-dimensional "target"

surfaces for the associated contact elements (CONTA173 in this case). Based on a sensitivity analysis, the application of such contact details led to FE load-displacement curves that better matched the experimentally obtained ones.

For each of the four fillet-welded CHS-to-CHS T-connection models discussed in this section (for the purpose of FE modelling verification), the modelled weld leg size was selected to produce a constant average throat size that was the same as the average of the measured values reported by Yang and Tousignant (2022).

For PJP groove welds, AWS D1.1-20 (AWS 2020) states that the effective throat is the shortest distance from the root to the face of a diagrammatic weld (i.e., the same as for fillet welds). For the seven PJP-welded CHS-to-CHS T-connection models discussed in this section (for the purpose of FE modelling verification), the PJP welds were modelled using a constant throat size around the perimeter of the welded joint with a bevel angle of $\phi = 60°$, as shown in Fig. 3.5. The modelled weld throat sizes were the averages of the measured values reported by Yang and Tousignant (2022).

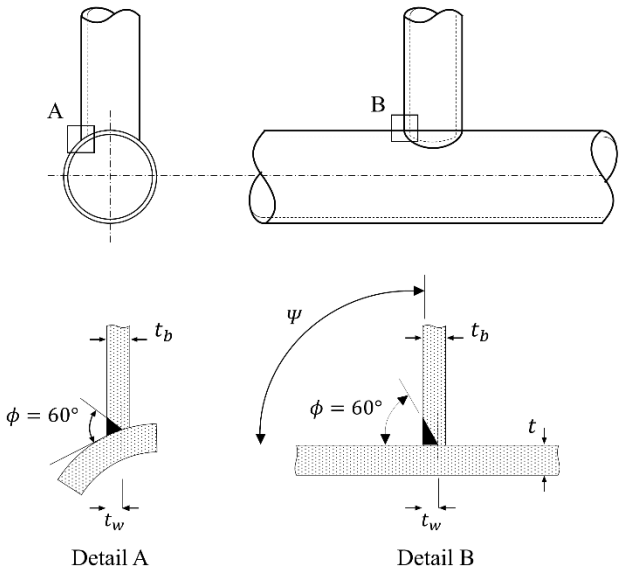

Fig. 3.5. PJP welds detail and joint nomenclature

It was found that the introduction of contact (Fig. 3.5) had a negligible effect on the load-deformation response for the PJP-weld connections because, different from the fillet-welded connections, the gap between the branch and chord members are much narrower than the branch wall thickness (Fig. 3.5). It should be noted that for matched connections (i.e., $\beta = 1.0$), ϕ was not 60° but complied with AWS D1.1 (2020) and CSA W59 (2018) as a "flare bevel groove weld" to produce a constant weld throat size.

3.4 Weld Fracture Criterion

For the FE simulation work presented in this study, the weld fracture criterion recommended by Voth and Packer (2012), Tousignant and Packer (2018) and Yaghoubshahi et al. (2019) was applied. This approach utilizes the element death feature in ANSYS (2021). When an element reaches a predefined fracture equivalent strain (ε_{ef}), the ANSYS death feature reduces the stiffness of the element to near-zero and hence the element carries near-zero stress and becomes inactive. The pre-fracture load carried by the deactivated element is then transferred to the adjacent elements, and the deactivated element is allowed to deform freely. This process is repeated for each displacement-controlled load step in an iterative manner, with an increasing number of weld elements being deactivated to simulate crack development, until the final connection failure.

As discussed in Section 3.1, for the connection tests reported by the Yang and Tousignant (2022), for calculation of the magnitude of the branch in-plane bending moment, the branch length (l_b), which is the distance between the line of application of the horizontal displacement and the welded joint, was multiplied by the horizontal force (P). All branch lengths (l_b) used in the FE analysis were the same as those in the experimental tests. To determine a suitable value for the fracture equivalent strain (ε_{ef}), the experimental data from the 11 connections was used, including

the actual weld strength (M_a = the maximum moment resistance of the welded joint) and the branch in-plane displacement. The experimentally data is compared to the numerically obtained weld strength (M_{FE}) and branch in-plane displacement. Sample comparisons for six connections are shown in Fig. 3.6 where the ratios of the experimental-to-FE ratios of the bending moment and the branch in-plane displacement are plotted against different values of fracture equivalent strain (ε_{ef}). Based on the data from all 11 connections in Table 3.1 and the approach recommended by Voth and Packer (2012), Tousignant and Packer (2018) and Yaghoubshahi et al. (2019), the best-fit value for ε_{ef} was determined to be 0.25. This minimizes the error associated with the scatter and approaches the desired near-one experimental-to-FE ratios for both bending moment (at fracture of welded joint) and branch displacement. The averaged experimental-to-FE ratios of fracture moment and branch deflection for all 11 connections are 1.05 (COV = 0.10) and 0.99 (COV = 0.30), respectively. The reasonably good agreements between the experimental and numerical data gives credence to the FE modelling approach herein. The same fracture equivalent strain (ε_{ef}) value of 0.25 is used in further verification of the FE modelling approach in Section 3.5 and the subsequent FE parametric study in Section 4.

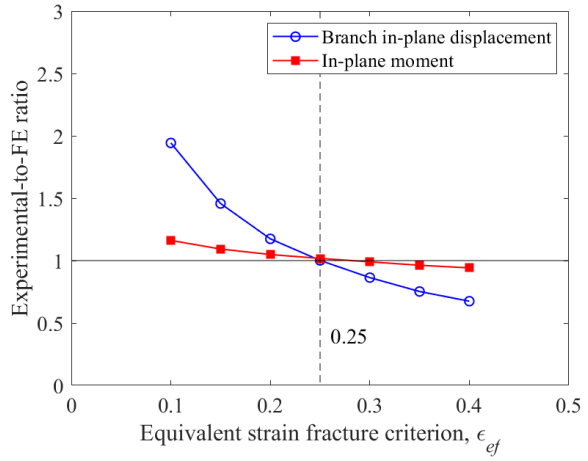

(a) T406-273-1P

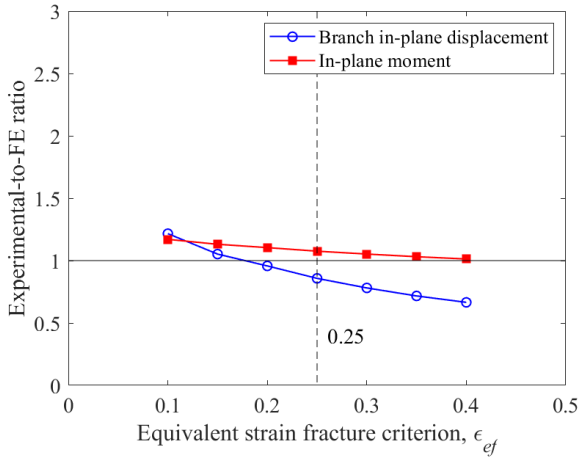

(b) T406-127-1F

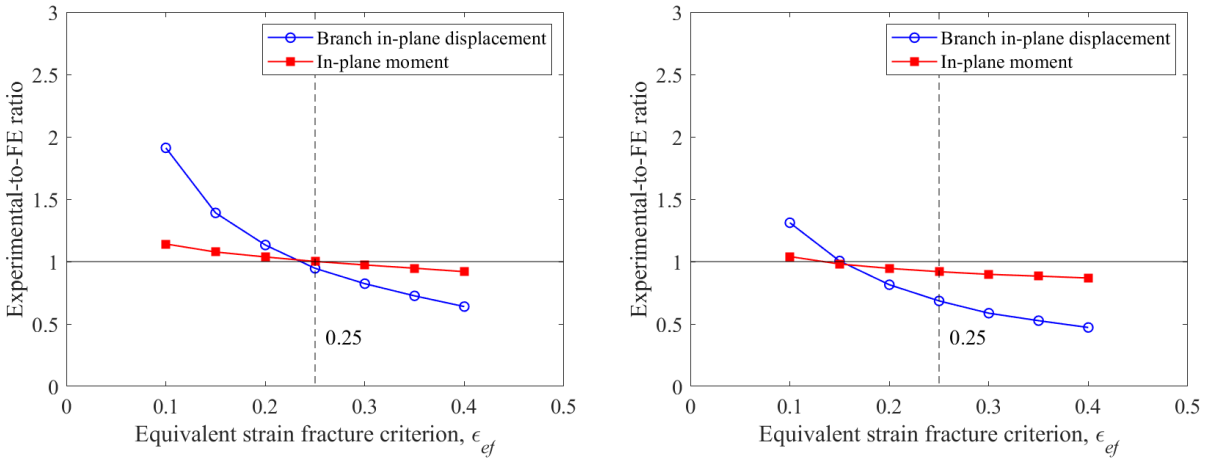

(c) T356-273-1P (d) T356-324-1P

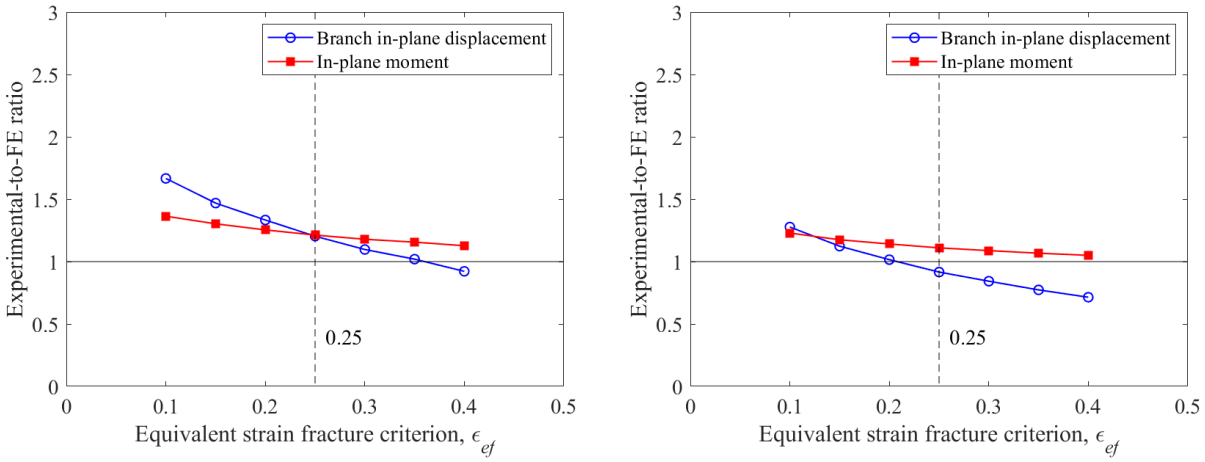

(e) T406-127-0.7F (f) T356-127-1F

Fig. 3.6. Experimental-to-FE ratios of applied moment and branch displacement for different equivalent strain (ε_{ef})-values for typical connections

3.5 Evaluation of FE Models Against Experimental Results

For the 11 CHS-to-CHS moment T-connection tests performed by Yang and Tousignant (2022), the connection responses under branch in-plane bending were captured using the applied moment-chord wall indentation plots. The branch deflections at different load levels were used to calculate the chord wall indentations throughout the connection tests until the connections failed by weld rupture. Using the ANSYS death feature and a predefined fracture equivalent strain (ε_{ef})-

value of 0.25, the complete applied moment-chord indentation curves can now be generated for the 11 FE connection models until failure by weld rupture. The objective is to evaluate the FE connection response curves against the experimental results in this section to verify the FE modelling approach.

For each connection test performed by Yang and Tousignant (2022), the horizontal deflection at the load application point on the branch (Δ_{total}) relative to the connection work points were recorded. The branch member flexural deflection was calculated ($\Delta_f = Pl_b^3/3EI_b$, where I_b is the moment of inertia of the branch cross-section). The branch member rigid body (Δ_{rigid}) deflection was determined by subtracting the total branch deflection (Δ_{total}) by the branch member flexural deflection (Δ_f). The branch indentation into the chord member at the crown point on the compression side (Δ_D) was determined using Eq. (12). Subsequently, Eq. (13) was applied to use the chord diameter to normalize the calculated chord wall indentation due to branch in-plane bending. Another objective (by applying Eq. (13) to normalize the chord indentation) is to allow for comparison of the normalized chord deformation (Δ_{norm}) at weld rupture to the widely accepted 3% chord deformation limit for tubular steel connection research (Yang and Tousignant 2022). The same was applied in the FE simulations in this research. The FE connection response curves are verified against the experimental results for all 11 connections in Fig. 3.7 where good agreements can be seen. Therefore, the FE modelling approach in this paper is deemed reliable and further credence can be given to the subsequent FE parametric study.

$$\Delta_D = \frac{\Delta_{rigid} D_b}{2 l_b} \tag{12}$$

$$\Delta_{norm} = \Delta_D / D \tag{13}$$

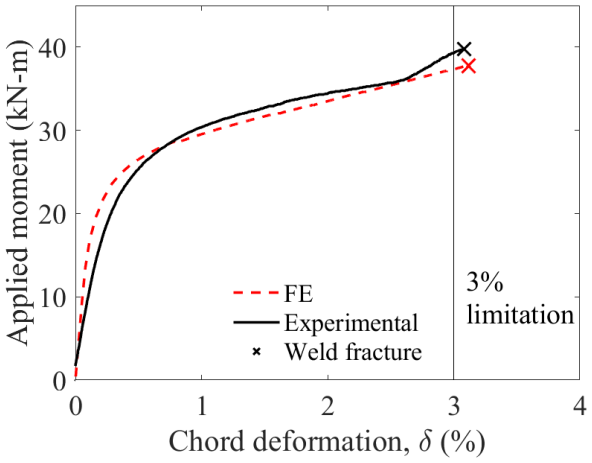

(a) T273-127-1P

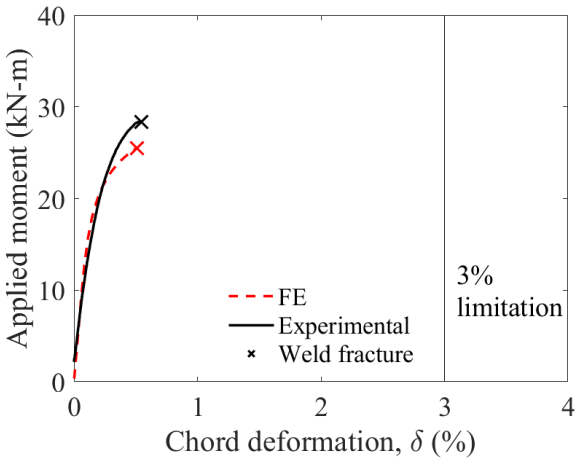

(b) T356-127-1F

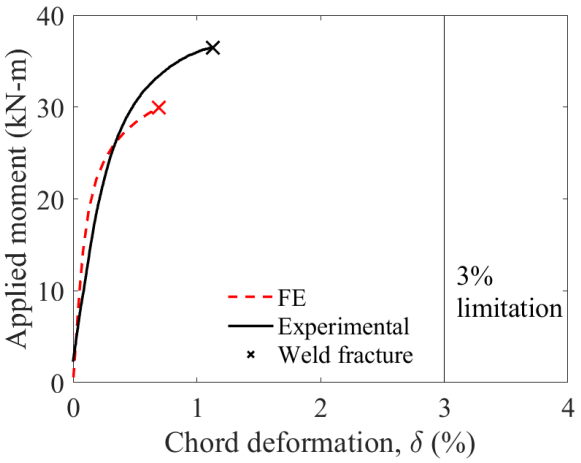

(c) T324-127-1F

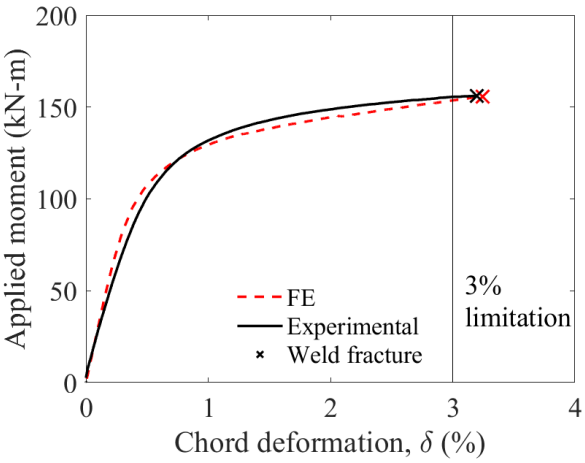

(d) T356-273-1P

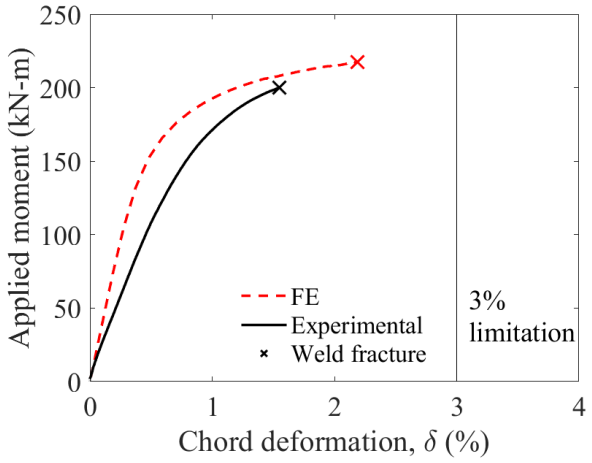

(e) T356-324-1P

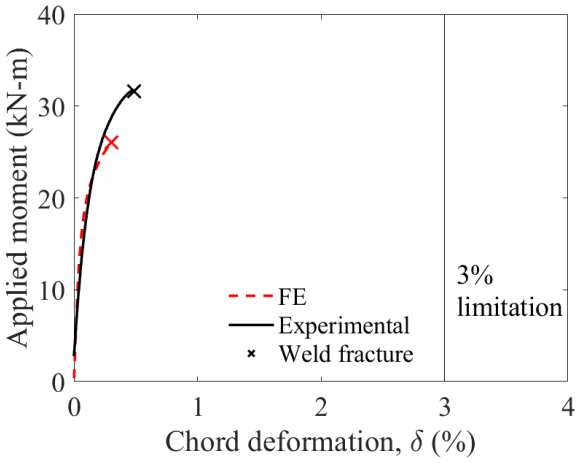

(f) T406-127-0.7F

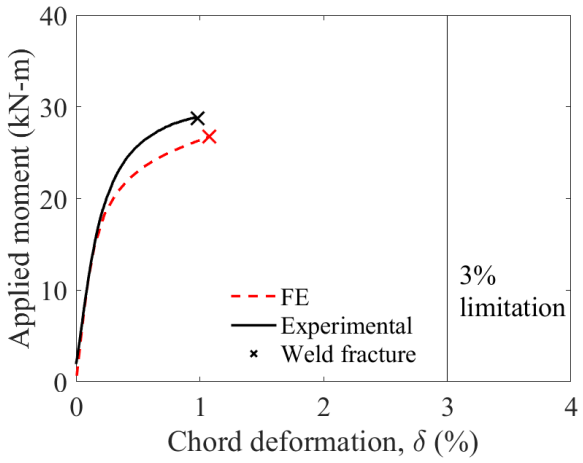

(g) T406-127-1F

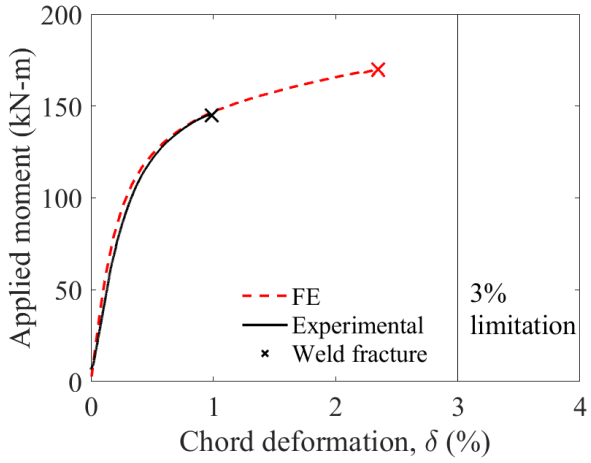

(h) T406-273-0.7P

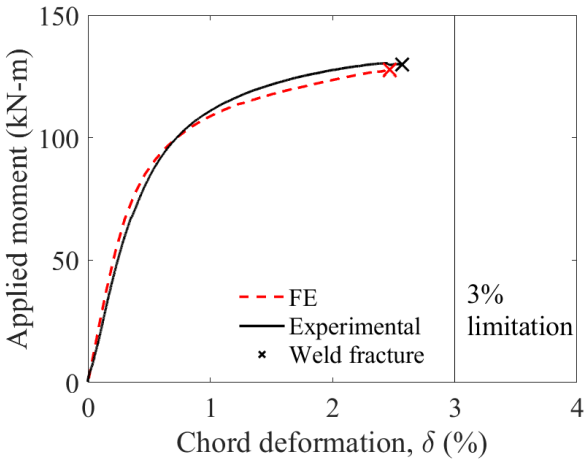

(i) T406-273-1P

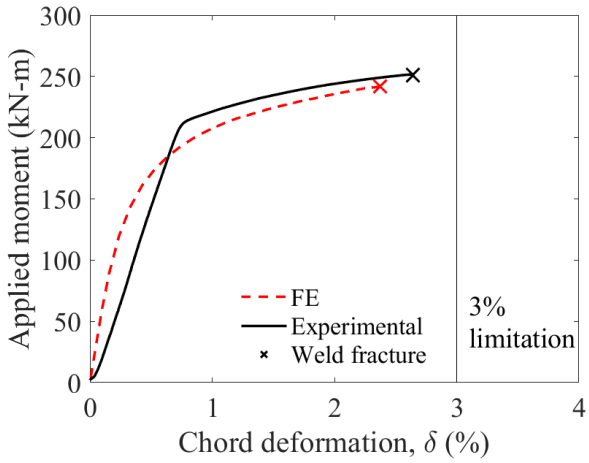

(j) T406-324-0.7P

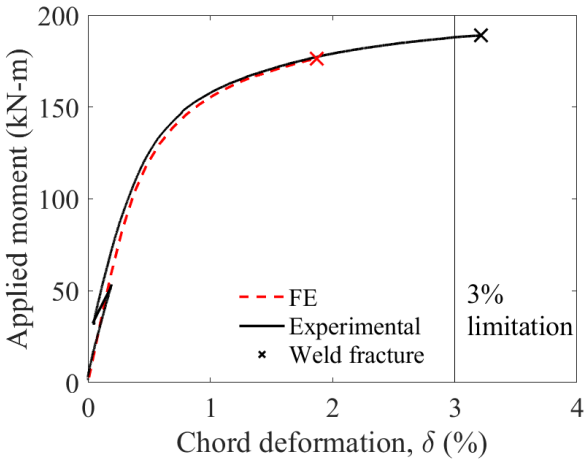

(k) T406-324-1P

Fig. 3.7. Applied moment versus chord deformation of 11 connections

Further analysis was performed by comparing the strain distribution along the circumference of the branch. Unidirectional strain gauges (SGs) oriented along the branch axis were set up to measure the normal strain distribution. The SGs were placed evenly around half of the branch circumference due to symmetry and 15mm above the weld to avoid the notch effect due to the sudden change in geometry (Packer & Cassidy, 1995). The experimentally measured strain data from the SGs were evaluated by the elastic strain obtained from FE at the same location as the SGs. The strain distribution was measured under different in-plane bending moment with the subtended angle (ρ) from 0° (toe, the compression side) to 180° (heel). Fig. 3.8 compares FE and experimental strain distributions under $0.25M_a$ (25% of the experimental fracture moment) and $0.9M_a$ for two typical connections. When the applied moment is relatively low ($0.25M_a$), the strain distributions fit well for FE and experimental tests. However, when the applied moment reaches $0.9M_a$, the FE strain distributions differ significantly from the experimental strain distributions. This is because of the non-uniform yielding of the weld along its length due to non-uniform weld geometry in experimental tests, which does not occur in FE programs. Also, the strain distributions in the tensile side (90° – 180°) of the branch match better than those in the compression side (0° − 90°). In general, the FE and experimental strain distributions show the same variation trend, which proves the validation of the FE models. Both experimental and FE results show the uniform strain distribution that the peak strain is not located at ρ = 0° or 180°. This finding was also corroborated in FE that the initial “death” elements were not detected at the crown or saddle of connections but at the intermediate part between the crown and saddle, where the crack starts to initiate and propagate. Therefore, the FE modelling approach in this paper is deemed convincing and reliable.

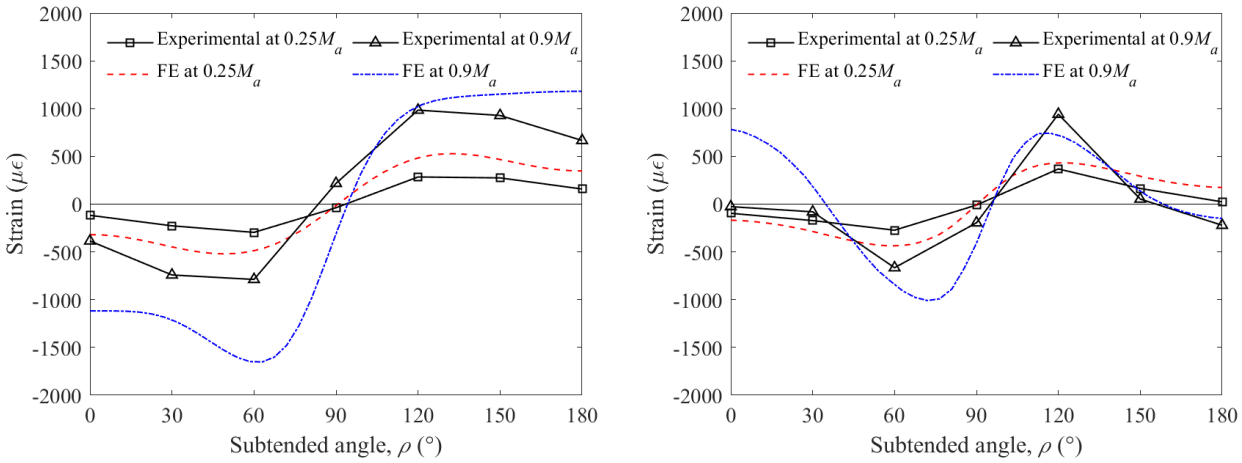

(a) T324-127-1F (b) T406-324-0.7P

Fig. 3.8. Comparison of FE and experimental strain distributions under different load levels

Chapter 4: Finite Element Parametric Study

4.1 Model Size Effect Analysis (Scalability)

The purpose of the parametric study is to study the effects of the non-dimensional connection parameters (β, τ, and $2\gamma = D/t$) on the behaviours of the welded joints. First, a series of FE models with the same non-dimensional parameters but different chord diameters were developed and analysed (before the main parametric study) to study the model size effect (scalability). The FE results are summarized in Table 4.1, where $M_{n\text{-}ip}$ is the in-plane fracture moment calculated by Eq. (2) and M_{FE} is the in-plane fracture moment obtained in the FE analysis. The normalized connection strength ($M_{FE}/M_{n\text{-}ip}$) is found to be unaffected by different absolute model sizes, and the results of the parametric study are hence considered applicable for connections with the same non-dimensional connection parameters.

Table 4.1. Scalability analysis results

D(mm)	β	τ	2γ	$M_{n\text{-}ip}$	M_{FE}	$M_{FE}/M_{n\text{-}ip}$
100	0.55	1.0	50	0.84	1.15	1.37
200	0.55	1.0	50	6.69	9.03	1.35
300	0.55	1.0	50	22.58	30.71	1.36
400	0.55	1.0	50	53.53	72.17	1.35

4.2 Range of Parameters

The ranges of parameters were carefully chosen to maintain a broad scope of the parametric study. The non-dimensional parameters were selected as: the branch-to-chord diameter ratio (β) = 0.40, 0.55, 0.70, 0.85, and 1.00; the branch-to-chord thickness ratio (τ) = 0.20, 0.30, 0.40, 0.50, 0.60, 0.70, 0.80, 0.90, and 1.00; the chord slenderness ratio ($2\gamma = D/t$) = 10, 20, 30, 40, and 50;

and the branch inclination angle = 90°. The combination of such parameters led to 225 permutations. However, Table K4.1A of AISC 360-22 (AISC 2022) specifies that CHS-to-CHS moment connections need to have $D_b/t_b \leq 0.05E/F_{yb}$ to prevent premature member buckling. A total of 104 permutations (out of 225) satisfies the AISC requirement. Based on the 104 permutations, 33 fillet-welded FE connection models (β = 0.40) and 104 PJP-welded FE connection models (β = 0.40, 0.55, 0.70, 0.85, and 1.00) were created and analyzed.

4.3 Details of Parametric Models

All 137 FE connection models had the same chord diameter of 300 mm. The other connection dimensions varied with the selected nondimensional design parameters. For both fillet welds and PJP welds, the weld throat size was set to $0.5t_b$ to ensure that the weld fracture occurs before the branch yielding. The length of the chord (l) was $10D$ (when $D/t > 25$) or $6D$ (when $D/t \leq 25$) to avoid the chord end effect (Van der Vegte and Makino 2010). The length of the branch (l_b) was $3D_b$ to eliminate the branch length effect (Mehrotra and Govil 1972). The same set of material properties for the chord, branch and weld materials are used for all models in the parametric study. The material properties are obtained from the tensile coupon tests performed by Yang and Tousignant (2022). The key material characteristics of this set best matched the nominal values. The key material characteristics are summarised in Table 4.2, and the engineering stress-strain curves of the branch, chord and weld materials are plotted in Fig. 4.1.

Table 4.2. Key material characteristics

	E (MPa)	F_y (MPa)	F_u (or F_{EXX}) (MPa)
Chord	196000	382	492
Branch	198000	352	475
Weld	208000	534	587

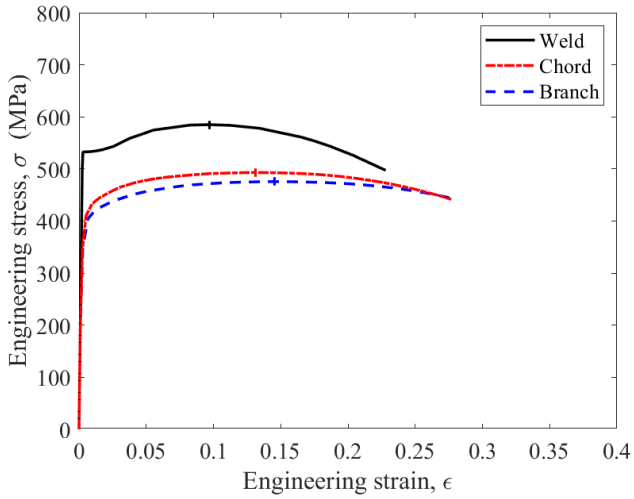

Fig. 4.1. Engineering stress-strain relationships used in parametric study

The previously determined fracture equivalent strain (ε_{ef}) of 0.25 was applied to the weld materials in all FE models to trigger the ANSYS death feature (ANSYS 2021) to simulate crack initiation and propagation. The load application and connection boundary conditions are the same as those used in the FE modelling verification work. As done in the FE modelling verification work, only one half of the connection is modelled to save computational time. Therefore, for the following analysis, the horizontal force on the branch in the FE analysis was multiplied by a factor of two and further multiplied by the branch length (l_b) to determine the bending moment for the full connection (M_{FE}).

Chapter 5: Results and Evaluation of Parametric Study

As expected, all 137 parametric models failed by weld rupture (weld-critical) and hence the data was used in the following analysis on the behaviour of welded joints in CHS-to-CHS moment T-connections under branch in-plane bending. The normalized chord deformation (i.e., chord indentation under branch in-plane bending = $\Delta_{norm} = \Delta_D/D$) was determined using the approach discussed in Section 3.5. For all models, the Δ_{norm}-values ranged from 0.19% to 3.75% when the connections failed by weld rupture. For six of the 137 FE models, the weld rupture occurred after the chord deformation limit (Δ_D/D = 3%).

As discussed in the Section 1, Yang and Tousignant (2022) developed a preliminary formula for calculation of the weld effective elastic section modulus based on the available yet limited experimental data (four fillet-welded and seven PJP-welded connections). In this section, the accuracy of the preliminary approach for strength prediction of the welded joints (i.e., the applications of Eqs. (2), (4), (5) and (8)) is examined using the newly generated FE data before further development of a new and more robust approach.

Using Eqs. (2), (4), (5) and (8), the material properties in Table 4.2 and the FE connection dimensions, the nominal strengths of the welded joints ($M_{n\text{-}ip}$) were calculated and compared to the FE weld fracture moment (M_{FE}) in Fig. 5.1. The results for the fillet-welded and PJP-welded connections are shown separately in the figure for clearer inspection.

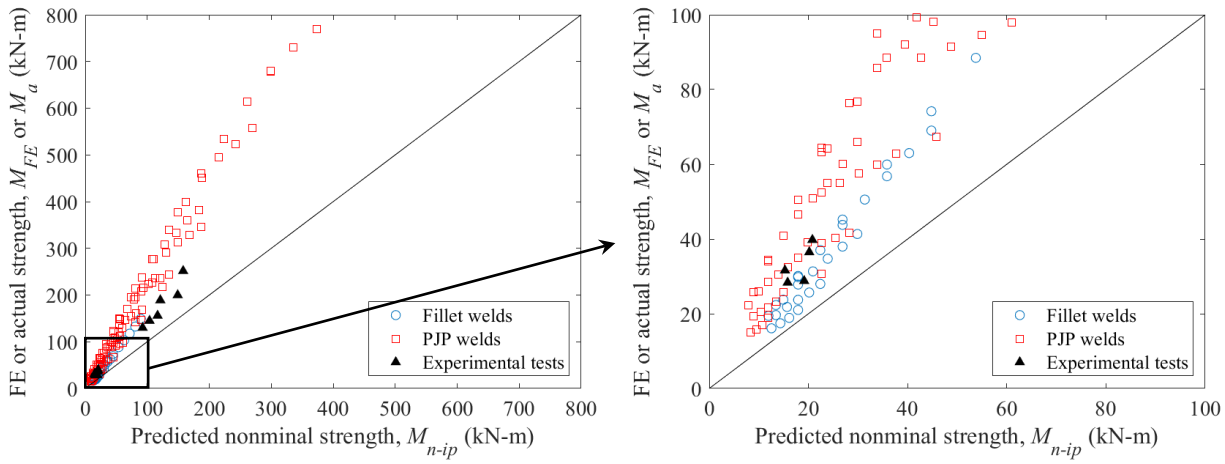

Fig. 5.1. Actual-to-predicted weld strength ratios using Eqs. (2), (4), (5) and (8)

For the fillet-welded connections shown in Fig. 5.1, the average value of the FE-to-predicted weld fracture moment ratios ($M_{FE}/M_{n\text{-}ip}$) is 1.51, and the COV is 0.11. As discussed in Section 3.1, for all FE models, to ensure that the load transfer from the branch to the chord was only through the weld at the initial stage, a gap of 0.25 mm was modelled between the two members at the joint location. The FE parametric analysis in this research showed that a part of the applied branch in-plane bending moment is resisted by direct bearing of the branch on the chord connecting face at the compressive side of the welded joint when the applied load increases. This mechanism was observed by careful examination of the FE contact elements. Hence, the rupture of the welded joint was delayed by the bearing mechanism (which is consistent with findings from Yahoubshahi et al.'s (2019) research on fillet welds in RHS-to-RHS moment T-connections under branch in-plane bending). It should be noted that the preliminary approach proposed by Yang and Tousignant (2022) does not consider the bearing mechanism (because it is not practical to measure), and questions also exist as to whether it can be relied on (Tousignant and Packer 2020b). Nonetheless,

for the fillet-welded connections the average value of the FE-to-predicted weld fracture moment ratios ($M_{FE}/M_{n\text{-}ip}$) is much greater than unity, and a more accurate approach may be warranted.

For the PJP-welded connections shown in Fig. 5.1, the average value of the FE-to-predicted weld fracture moment ratios ($M_{FE}/M_{n\text{-}ip}$) is 2.21, and the COV is 0.17. Hence, the preliminary approach is even more conservative for strength prediction of the PJP-welded joints (i.e., the applications of Eqs. (2), (5) and (8)). When the FE data from the fillet- and PJP-welded connections are combined, the average value of the FE-to-predicted weld fracture moment ratios ($M_{FE}/M_{n\text{-}ip}$) is 2.05 (COV = 0.22).

To investigate this further, the actual weld effective elastic section modulus based on the numerical analyses ($S_{FE\text{-}ip}$) for all FE models was calculated by dividing the numerically obtained moment at weld rupture (M_{FE}) by the F_{nw}-values calculated by Eqs. (4) and (5). Using the geometric properties of all FE models, the nominal weld effective elastic section moduli ($S_{n\text{-}ip}$) were calculated by Eq. (8) (i.e., the formula proposed by Yang and Tousignant 2022). The $S_{FE\text{-}ip}/S_{n\text{-}ip}$-ratios are plotted against the β, τ and 2γ in Fig. 5.2. Close examination of Fig. 5.2 allows one to determine:

(i) the specific conditions under which Eq. (8) becomes excessively conservative; and

(ii) the effects of different nondimensional parameters on the behaviours of fillet- and PJP-welded joints.

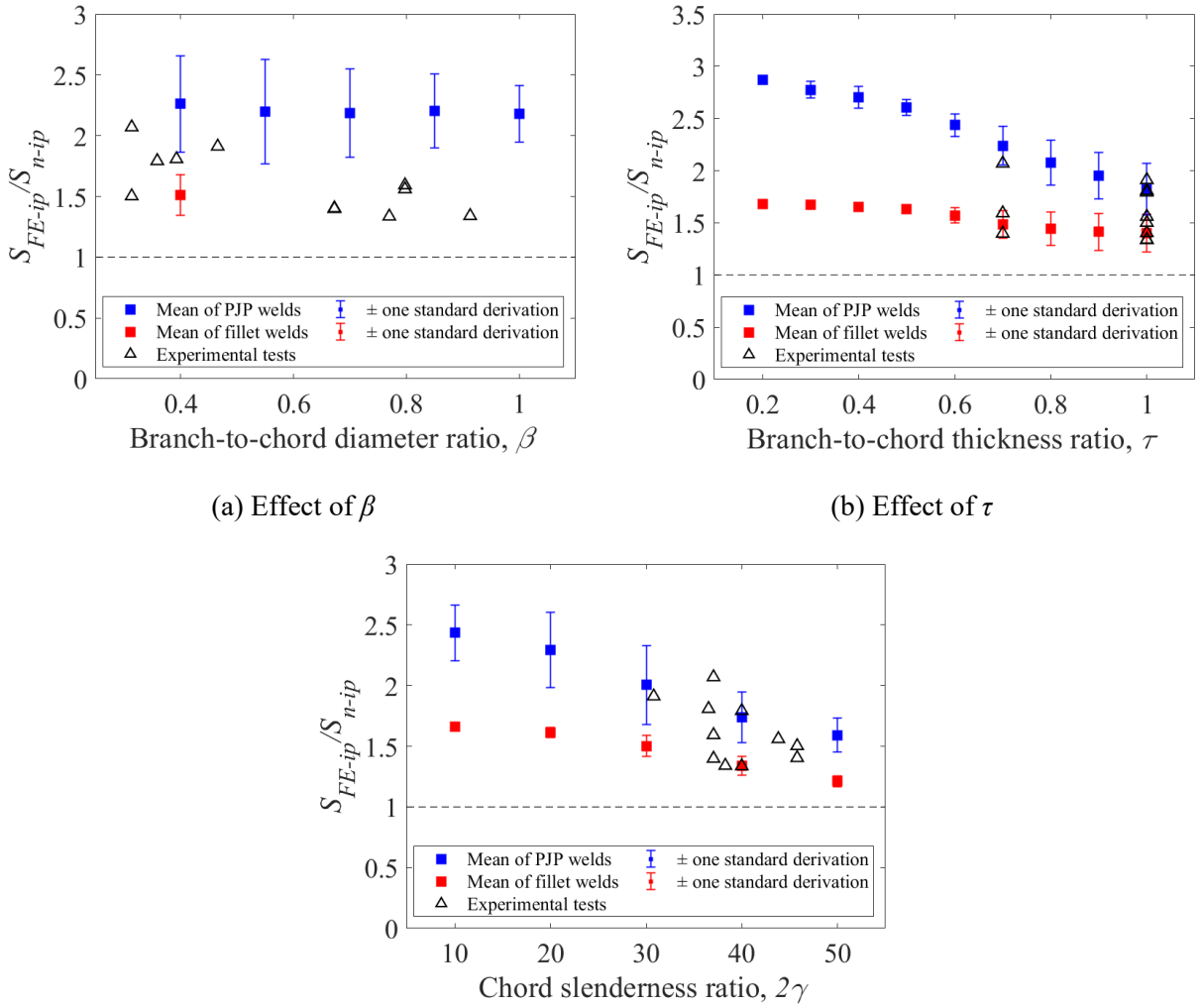

(a) Effect of β

(b) Effect of τ

(c) Effect of 2γ

Fig. 5.2. Effect of non-dimensional parameters on weld effective elastic section modulus $S_{FE\text{-}ip}/S_{n\text{-}ip}$

Based on Fig. 5.2, it is apparent that:

(i) As β increases, the FE-to-predicted section modulus ratio does not change significantly for PJP welds. In other words, $S_{FE\text{-}ip}$ remains relatively constant due to the trade-off between an increasing weld length and a decreasing (in a relative sense) weld effective section modulus.

(ii) As τ increases, the FE-to-predicted section modulus ratio decreases, which is more obvious for PJP welds. The increase in τ reflects an increase in t_b and t_w insofar as this parametric study was concerned (i.e., t was held constant). Thus, at weld fracture, greater chord deformation, less uniform stress in the weld, and a lower weld strength are observed in connections with higher τ.

(iii) As 2γ increases, the FE-to-predicted section modulus ratio decreases for both PJP welds and fillet welds. The increase in 2γ also leads to greater chord deformation, less uniform stress in the weld, and a lower weld strength.

Chapter 6: Proposal of New Weld Design Method

In AISC 360-22 (AISC 2022), Table K5.2 includes the formulae for determination of l_e in CHS-to-CHS T-, Y- and X-connections under branch axial force. It should be noted that the new Table K5.2 caters only to fillet-welded connections with $\beta \leq 0.50$ and further research is currently being performed to extend this limit of validity.

Based on the forgoing analysis, which covered fillet-welded connections with $0.2 \leq \beta \leq 0.5$ and PJP-welded connections with $0.2 \leq \beta \leq 1.0$, it would seem reasonable that Yang and Tousignant's (2022) Eq. (8) for S_{ip} be modified to:

$$S_{ip} = \left(1 + \frac{1}{\sqrt{\tau\gamma}}\right) t_w \frac{(3 + 1/\sin\theta)}{4 \sin\theta} \pi \left(\frac{D_b}{2}\right)^2 \tag{14}$$

The proposed Eq. (14) includes the factors τ and γ, and – as shown in Section 7 – provides an adequate level of reliability when used in conjunction with Eqs. (2), (4) and (5) to calculate $M_{n\text{-}ip}$. Fig. 6.1 shows the correlation of the new $S_{FE\text{-}ip}/S_{n\text{-}ip}$-ratios calculated with Eq. (14) against β, τ and 2γ.

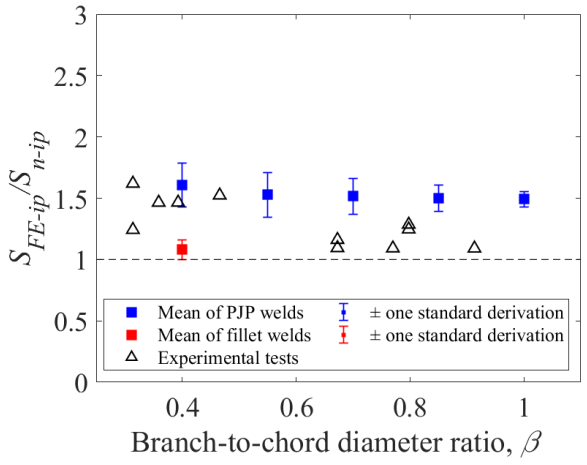

(a) Effect of β

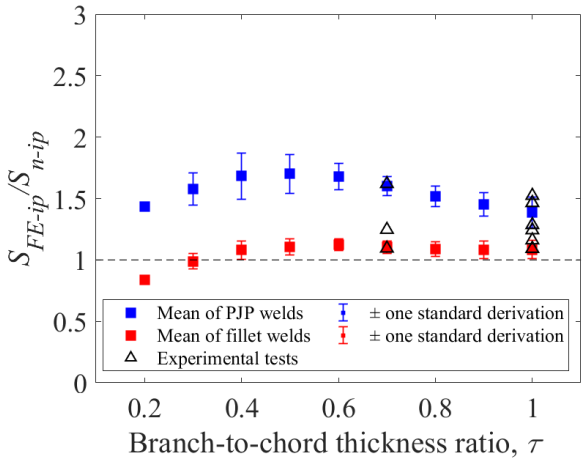

(b) Effect of τ

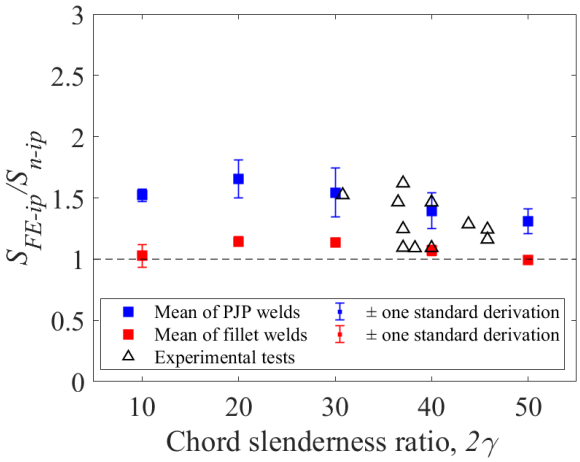

(c) Effect of 2γ

Fig. 6.1. Effect of non-dimensional parameters on weld effective elastic section modulus $S_{FE\text{-}ip}/S_{n\text{-}ip}$ using Eq. (14)

Chapter 7: Evaluation of Proposed Design Method

7.1 Reliability Analysis Based on FORM

To evaluate the proposed new weld design method, an approximate first-order reliability method (FORM) analysis was performed to determine the safety index β^+, using Eq. (15) (Schmidt and Bartlett 2002):

$$\beta^+ = \frac{1}{\sqrt{V_R^2 + V_S^2}} ln\left[\frac{\delta_R}{\phi}\left(\frac{\gamma_D + \gamma_L(L/D)}{\delta_D + \delta_L(L/D)}\right)\right] \quad (15)$$

where δ_R = bias coefficient for the resistance; V_R = COV of δ_R; γ_D and γ_L = load factors for dead and live loads, respectively; δ_D and δ_L = bias coefficients for dead and live loads, respectively; L/D is the ratio of live-to-dead load; and V_S = COV of the total load effect, according to CSA S6:19 (CSA 2019b):

$$V_S = \frac{\sqrt{(\delta_D V_D)^2 + [\delta_L V_L (L/D)]^2}}{\delta_D + \delta_L(L/D)} \quad (16)$$

where V_D and V_L = COV of dead and live loads, respectively.

Eqs. (15) and (16) include the effects of the load variation by considering the dead and live loads. The bias coefficients and COVs in the equations were taken as δ_D = 1.05 and V_D = 0.10 for the dead load, and δ_L = 0.78 and V_L = 0.32 for the live load (Schmidt and Bartlett 2002). The load factors were chosen as γ_D = 1.2 and γ_L = 1.6 according to ASCE 7-16 (ASCE 2016). The ratio of live-to-dead load (L/D) was taken as $1 \leq L/D \leq 3$ to be consistent with previous research on steel structures (e.g., MacPhedran and Grondin 2011; Tousignant et al. 2022).

The distribution of the resistance is lognormal if the component factors are independent of each other, and the bias coefficient δ_R and its COV V_R are given by (Kwan et al. 2010; Schmidt and Bartlett 2002) as:

$$\delta_R = \delta_G \delta_M \delta_P \delta_d \tag{17}$$

$$V_R = \sqrt{V_G^2 + V_M^2 + V_P^2 + V_d^2} \tag{18}$$

where δ_G, δ_M, δ_P, δ_d are the bias coefficients of the geometric, material, professional, and discretization factors, and V_G, V_M, V_P, V_d are the associated COVs. Specifically for this paper, δ_G incorporates variability in weld throat size; δ_M incorporates variability in electrode strength; δ_P incorporates variability in the accuracy of the design equation used to calculate $M_{n\text{-}ip}$; and δ_d incorporates the effect of specifying discrete and commonly used weld throat sizes that are generally more than the capacity of the load and resistance factor design (LRFD) requirements.

The target value of β^+ was taken as 4.0 for connection design, in accordance with Chapter B of the AISC 360-22 Commentary (AISC 2022). The resistance factors were taken as ϕ = 0.75 for fillet welds and ϕ = 0.80 for PJP welds, in accordance with Table J2.5 of AISC 360-22. In this section, the analysis is also performed using ϕ = 0.80 (conservatively) for all welds (i.e., fillet + PJP in Table 7.1).

The parameters δ_G and V_G were taken as 1.03 and 0.10, respectively, from a large database of pre-test measurements of weld profile and the nominal weld leg size to reflect fabrication error in weld geometry (Callele et al. 2009). The parameters δ_M and V_M were taken as 1.12 and 0.077, respectively, based on a large collection of weld metal tensile tests (Lesik and Kennedy 1990). The parameters δ_d and V_d were taken as 1.09 and 0.062, respectively, which were adopted from previous research on fillet welds (Thomas and Tousignant 2022). The parameters for PJP welds were similar and were also used in (Yang and Tousignant 2022). The professional factors δ_P and

V_p were dependent on different weld types and design methods. The bias coefficients δ_P and COVs V_p are summarized in Table 7.1. for fillet welds, PJP welds, and all welds together.

Table 7.1. Reliability analysis parameters

Weld type	Bias coefficient and Coefficient of Variation			
	δ_P	V_P	δ_R	V_R
Fillet	1.121	0.129	1.409	0.191
PJP	1.522	0.118	1.913	0.183
Fillet + PJP	1.421	0.172	1.787	0.222

The data from the 11 connection tests from Yang and Tousignant (2022) and the 137 FE models from this research were included in the reliability analysis. The safety index β^+ was calculated for $1 \leq L/D \leq 3$ and different ϕ-values for different weld types, using Eq. (15).

7.2 FORM Analysis Results

Table 7.2 shows the ranges of β^+-values for different target ϕ, including fillet welds ($\phi = 0.75$), PJP welds ($\phi = 0.80$), and fillet+PJP welds ($\phi = 0.80$) from the FORM analysis. For fillet welds, β^+ ranges from 4.09 to 4.37. For PJP welds, β^+ ranges from 5.00 to 5.50. For all welds (fillet+PJP), β^+ ranges from 4.37 to 4.61. In all cases, the target β^+-values of 4.0 is achieved. The distribution of β^+-values for different L/D-ratios are shown in Fig. 7.1(a) for different weld types for the proposed new weld design approach (i.e., the applications of Eqs. (2), (4), (5), (14)). For comparison purposes, the distribution of β^+-values for different L/D-ratios are shown in Fig. 7.1(b) for the preliminary weld design approach proposed by Yang and Tousignant (2022) (i.e., the applications of Eqs. (2), (4), (5) and (8)). The discontinuity of the curves is the intersection point of the pure dead load ($1.4D$) and the combination of dead load and live load ($1.2D + 1.6L$). As

shown in Fig. 7.1, the new approach better predicted the weld strengths of the connection specimens and FE models.

Using the newly proposed approach, the actual-to-predicted weld strength of the CHS-to-CHS moment T-connections under branch in-plane bending are shown in Fig. 7.2. For the fillet and PJP welds, the average value of the FE-to-predicted weld fracture moment ratios ($M_{FE}/M_{n\text{-}ip}$) are 1.12 (COV = 0.13) and 1.52 (COV = 0.12), respectively. Considering all welds, $M_{FE}/M_{n\text{-}ip}$ = 1.42 (COV = 0.17). Therefore, the new approach produces accurate predictions of the weld strengths and sufficient safety margins are achieved.

Table 7.2. FORM analysis results for 1⩽ L/D⩽ 3

	Range of β^+ for target ϕ
Fillet (ϕ = 0.75)	4.09-4.37
PJP (ϕ = 0.80)	5.00-5.50
Fillet+PJP (ϕ = 0.80)	4.37-4.61

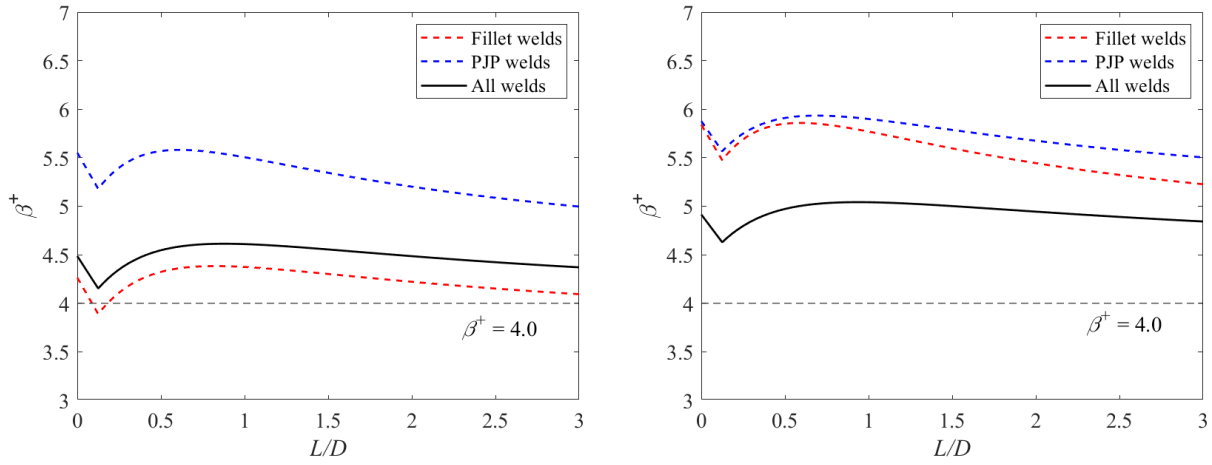

(a) β^+ of the newly proposed method

(b) β^+ of the method proposed by Yang and Tousignant (2022)

Fig. 7.1. Distribution of β^+-values for different *L/D*-ratios

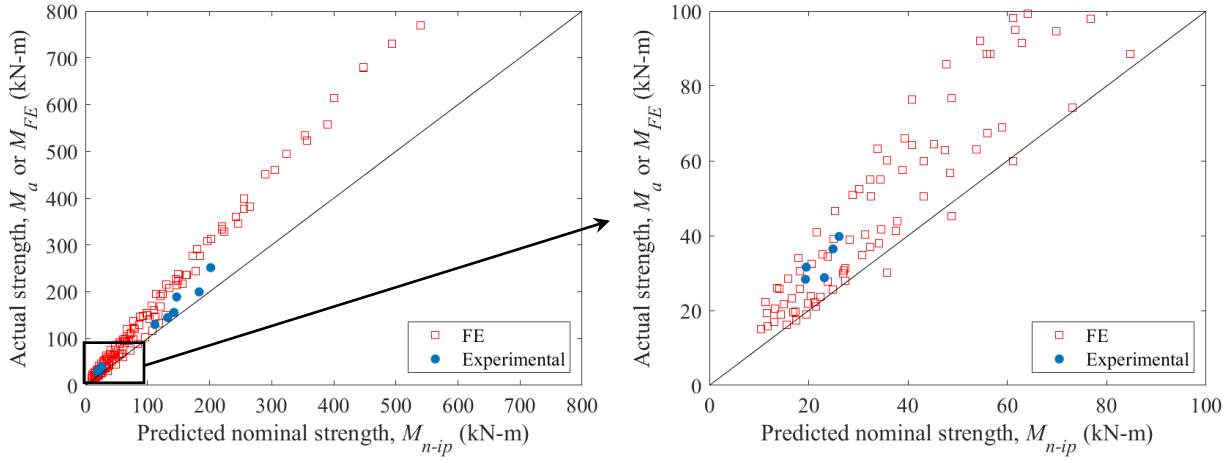

(a) (b)

Fig. 7.2. Actual-to-predicted weld strength ratios using the proposed method

Chapter 8: Conclusion

Chapter K of the current American Steel Design Specification (AISC 360-22) includes the effective length approach for design of welds in circular hollow section (CHS)-to-CHS T-, Y- and X-connections under branch axial force. Previous research effort has led to the development of new recommendation for CHS-to-CHS T-connections under branch in-plane bending. As a continuation of the recent effort, this research developed a new effective length approach for design of fillet and PJP welds in CHS moment T-connections under branch in-plane bending, based on a comprehensive FE parametric analysis and previous experimental data from full-sized connection tests. The newly proposed approach was shown to provide accurate strength predictions and achieve sufficient safety margins based on a first-order reliability method analysis. Future work can be concentrated on weld effective properties in other types of CHS-to-CHS connections.

Appendix A: Notation

The following symbols are used in this paper:

D	diameter of CHS chord
D_b	diameter of CHS branch
E	Young's modulus
F_{EXX}	ultimate stress of weld metal
F_{nw}	nominal weld strength
F_u	ultimate stress of CHS metal
F_y	yield stress
F_{yb}	yield stress of CHS branch
I_b	moment of inertia of CHS branch cross-section
L/D	live-to-dead load ratio
M_a	Actual (experimental) weld fracture moment
M_{FE}	FE weld fracture moment
$M_{n\text{-}ip}$	nominal flexural strength of in-plane bending
$M_{n\text{-}op}$	nominal flexural strength of out-of-plane bending
P	total horizontal reaction force at branch height
P_n	nominal axial resistance
$S_{FE\text{-}ip}$	weld effective elastic section modulus back calculated in FE
S_{ip}	weld effective elastic section modulus for in-plane bending
S_{op}	weld effective elastic section modulus for out-of-plane bending
V_D	coefficient of variation for dead load
V_G	coefficient of variation for geometry factor
V_L	coefficient of variation for live load
V_M	coefficient of variation for the material factor
V_P	coefficient of variation for the professional factor
V_R	coefficient of variation for the resistance
V_S	coefficient of variation for the total load effects

V_d	coefficient of variation for discretization
l	length of the chord
l_b	length of the branch
l_e	weld effective length
l_w	weld total length
t	thickness of the chord
t_b	thickness of the branch
t_w	weld throat dimension
w	weighing factor
β	branch-to-chord diameter ratio
β^+	safety index
γ	half diameter-to-thickness ratio of the chord
γ_D	load factor for dead load
γ_L	load factor for live load
Δ_D	chord indentation
Δ_{FE}	normalized FE chord indentation
Δ_a	normalized actual (experimental) chord indentation
Δ_f	flexural deflection of the branch
Δ_{norm}	normalized chord indentation
Δ_{rigid}	rigid body deflection of the branch
Δ_{total}	total deflection of the branch
δ_D	bias coefficient for dead load
Δ_{FE}	normalized FE chord indentation
δ_G	bias coefficient for the geometry factor
δ_L	bias coefficient for live load
δ_M	bias coefficient for the material factor
δ_P	bias coefficient for the professional factor
δ_R	bias coefficient for the resistance
δ_d	bias coefficient for discretization
ε	engineering strain
ε_{ef}	equivalent strain fracture criterion

ε_T	true strain
ε_T'	true strain at the start of necking
θ	branch inclination angle; angle between the force and weld longitudinal axis
θ_b	angle between branch and chord members
ρ	subtended angle
σ	engineering stress
σ_T	true stress
σ_T'	true stress at the start of necking
τ	branch-to-chord thickness ratio
ϕ	bevel angle of PJP welds; resistance factor
Ψ	local dihedral angle

Appendix B: Reference List

American Institute of Steel Construction (AISC). 2022. ANSI/AISC 360–22. Specification for Structural Steel Buildings, American Institute of Steel Construction, Chicago, IL, USA.

ANSYS. 2021. ANSYS Mechanical APDL, release 2021 R2. Houston, TX, USA.

American Society of Civil Engineers (ASCE). 2016. Minimum design loads and associated criteria for buildings and other structures. ASCE 7-16, American Society of Civil Engineers.

American Welding Society (AWS). 2015. AWS D1.1/D1.1M:2015. Structural Welding Code – Steel, Miami, FL, USA.

American Welding Society (AWS). 2020. AWS D1.1/D1.1M:2020. Structural Welding Code – Steel, 24th ed, Miami, FL, USA.

Canadian Standards Association (CSA). 2018. CSA W59–18. Welded steel construction, Canadian Standards Association, Toronto, Canada.

Canadian Standards Association (CSA). 2019a. CSA S16–19. Design of Steel Structures, Canadian Standards Association, Toronto, Canada.

Canadian Standards Association (CSA). 2019b. CSA S6:19. Canadian Highway Bridge Design Code, Canadian Standards Association, Toronto, Canada.

Callele, L. J., Driver, R. G., and Grondin, G. Y. 2009. Design and behavior of multi-orientation fillet weld connections. Engineering Journal-American Institute of Steel Construction, 46(4), 257-272.

Frater, G. S., and Packer, J. A. 1992a. Weldment design for RHS truss connections. I: Applications. Journal of Structural Engineering, 118(10), 2784-2803.

Frater, G. S., and Packer, J. A. 1992b. Weldment design for RHS truss connections. II. Experimentation. Journal of Structural Engineering, 118(10), 2804-2819.

International Organization for Standardization (ISO). 2013. ISO 14346:2013 (E). Static Design Procedure for Welded Hollow Section Joints – Recommendations, International Organization for Standardization, Geneva, Switzerland.

Kwan , Y. K., Gomez, I. R., Grondin, G. Y., and Kanvinde, A. M. 2010. Strength of welded joints under combined shear and out-of-plane bending. Canadian Journal of Civil Engineering, 37(2), 250-261.

Lesik, D. F., and Kennedy, D. L. 1990. Ultimate strength of fillet welded connections loaded in plane. Canadian Journal of Civil Engineering, 17(1), 55-67.

Ling, Y. 1996. Uniaxial true stress-strain after necking. AMP Journal of technology, 5(1), 37-48.

Luyties, W. H., and Post, J. W. 1988. Local dihedral angle equations for tubular joints and related applications. Welding Journal, 67(4), 51-60.

MacPhedran, I., and Grondin, G. Y. 2011. A simple steel beam design curve. Canadian Journal of Civil Engineering, 38(2), 141-153.

McFadden, M. R., Sun, M., and Packer, J. A. 2013. Weld design and fabrication for RHS connections. Steel Construction, 6(1), 5-10.

Mehrotra, B. L., and Govil, A. K. 1972. Shear Lag Analysis of Rectangular Full-Width Tube Junctions. Journal of the Structural Division, 98(1), 287-305.

Packer, J. A., and Cassidy, C. E. 1995. Effective weld length for HSS T, Y, and X connections. Journal of Structural Engineering, 121(10), 1402-1408.

Packer, J. A., Sherman, D., and Lecce, M. 2010. Hollow Structural Section Connections. AISC Steel Design Guide vol. 24, American Institute of Steel Construction, Chicago, IL, USA.

Packer, J. A., and Sun, M. 2011. Fillet weld design for rectangular HSS connections. Engineering Journal-American Institute of Steel Construction, 48(1), 31-48.

Packer, J. A., Sun, M., and Tousignant, K. 2016. Experimental evaluation of design procedures for fillet welds to hollow structural sections. Journal of Structural Engineering, 142(5), 04016007.

Schmidt, B. J., and Bartlett, F. M. 2002. Review of resistance factor for steel: resistance distributions and resistance factor calibration. Canadian Journal of Civil Engineering, 29(1), 109-118.

Thomas, J. H., and Tousignant, K. 2022. Design of Single-Sided Fillet Welds under Transverse Load. Journal of Structural Engineering, 148(9), 04022118.

Tousignant, K., and Packer, J. A. 2015. Investigation of weld effective length rules for RHS overlapped K-connections. Tubular Structures XV, 357-364.

Tousignant, K., and Packer, J. A. 2017a. Fillet weld effective lengths in CHS X-connections. I: Experimentation. Journal of Constructional Steel Research, 138, 420-431.

Tousignant, K., and Packer, J. A. 2017b. Numerical investigation of fillet welds in HSS-to-rigid end-plate connections. Engineering Journal, American Society of Civil Engineers.

Tousignant, K., and Packer, J. A. 2018. Fillet weld effective lengths in CHS X-connections. II: Finite element modelling, parametric study and design. Journal of Constructional Steel Research, 141, 77-90.

Tousignant, K., and Packer, J. A. 2019a. Fillet welds around circular hollow sections: HENRY GRANJON PRIZE 2018 winner Category C: Design and Structural Integrity. Welding in the World, 63(2), 421-433.

Tousignant, K., and Packer, J. A. 2019b. Weld effective lengths for round HSS cross-connections under branch axial loading. Engineering Journal-American Institute of Steel Construction, 56(3), 173-186.

Tousignant, K., and Packer, J. A. 2020a. Optimized design of fillet welds for CHS joints according to EN 1993‐1‐8. Steel Construction, 13(1), 41-51.

Tousignant, K., and Packer, J. A. 2020b. Weld design for hollow structural section connections: application to Canadian Standards. Canadian Journal of Civil Engineering, 47(10), 1128-1144.

Tousignant, K., Tayyebi, K., and Sun, M. 2022. Reliability of Existing and Proposed North American Design Provisions for RHS Compression Members with Slender Elements. Journal of Structural Engineering, 148(8), 04022108.

Van der Vegte, G. J., and Makino, Y. 2010. Further research on chord length and boundary conditions of CHS T-and X-joints. Advanced Steel Construction, 6(3), 879-890.

Voth, A. P., and Packer, J. A. 2012. Branch plate-to-circular hollow structural section connections. I: Experimental investigation and finite-element modelling. Journal of structural engineering, 138(8), 995-1006.

Yaghoubshahi, M., Sun, M., and Tousignant, K. 2019. Design of fillet welds in RHS-to-RHS moment T-connections under branch in-plane bending. Journal of Constructional Steel Research, 159, 122-133.

Yang, Z., and Tousignant, K. 2022. Experimental tests on fillet and PJP welds in CHS moment T-connections. Journal of Constructional Steel Research, 196, 107405.Tousignant, K., and Packer, J. A. 2018. Fillet weld effective lengths in CHS X-connections. II: Finite element

modelling, parametric study and design. Journal of Constructional Steel Research, 141, 77-90.

Tousignant, K., and Packer, J. A. 2019a. Fillet welds around circular hollow sections: HENRY GRANJON PRIZE 2018 winner Category C: Design and Structural Integrity. Welding in the World, 63(2), 421-433.

Tousignant, K., and Packer, J. A. 2019b. Weld effective lengths for round HSS cross-connections under branch axial loading. ENGINEERING JOURNAL-AMERICAN INSTITUTE OF STEEL CONSTRUCTION, 56(3), 173-186.

Tousignant, K., and Packer, J. A. 2020a. Optimized design of fillet welds for CHS joints according to EN 1993-1-8. Steel Construction, 13(1), 41-51.

Tousignant, K., and Packer, J. A. 2020b. Weld design for hollow structural section connections: application to Canadian Standards. Canadian Journal of Civil Engineering, 47(10), 1128-1144.

Tousignant, K., Tayyebi, K., and Sun, M. 2022. Reliability of Existing and Proposed North American Design Provisions for RHS Compression Members with Slender Elements. Journal of Structural Engineering, 148(8), 04022108.

Van der Vegte, G. J., and Makino, Y. 2010. Further research on chord length and boundary conditions of CHS T-and X-joints. Advanced Steel Construction, 6(3), 879-890.

Voth, A. P., and Packer, J. A. 2012. Branch plate-to-circular hollow structural section connections. I: Experimental investigation and finite-element modelling. Journal of structural engineering, 138(8), 995-1006.

Yaghoubshahi, M., Sun, M., and Tousignant, K. 2019. Design of fillet welds in RHS-to-RHS moment T-connections under branch in-plane bending. Journal of Constructional Steel Research, 159, 122-133.

Yang, Z., and Tousignant, K. 2022. Experimental tests on fillet and PJP welds in CHS moment T-connections. Journal of Constructional Steel Research, 196, 107405.

Appendix C: Chord Indentation Formula for CHS-to-CHS Moment Connections

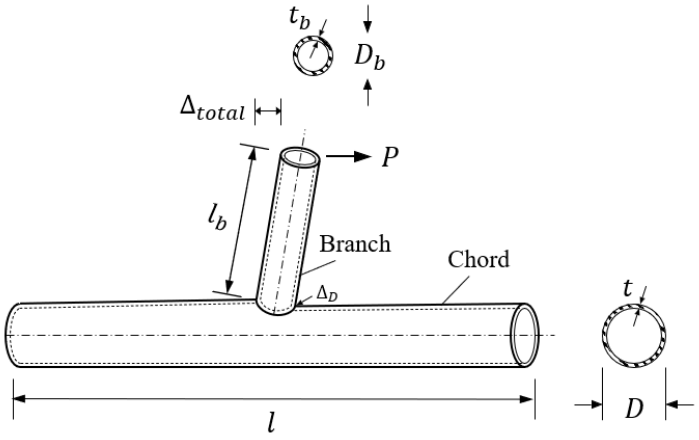

Fig. C.1. CHS-to-CHS moment connection geometry

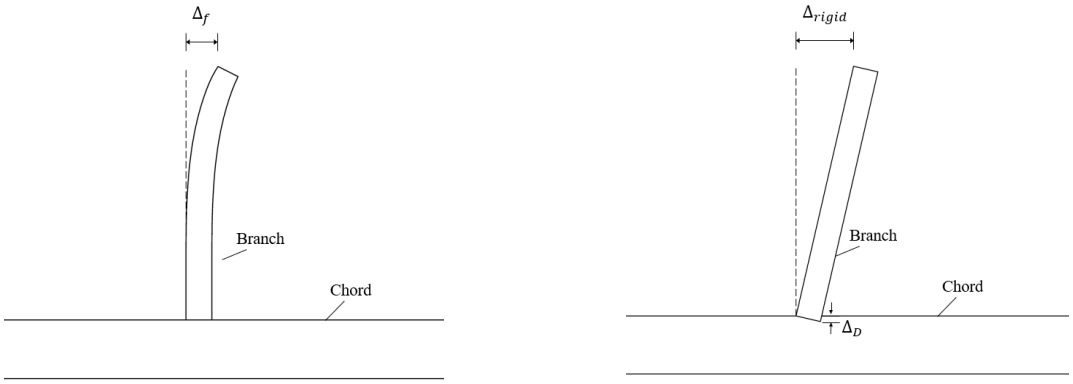

(a) Flexural deflection Δ_f (b) Rigid body deflection Δ_{rigid}

Fig. C.2. Branch in-plane deflection configuration

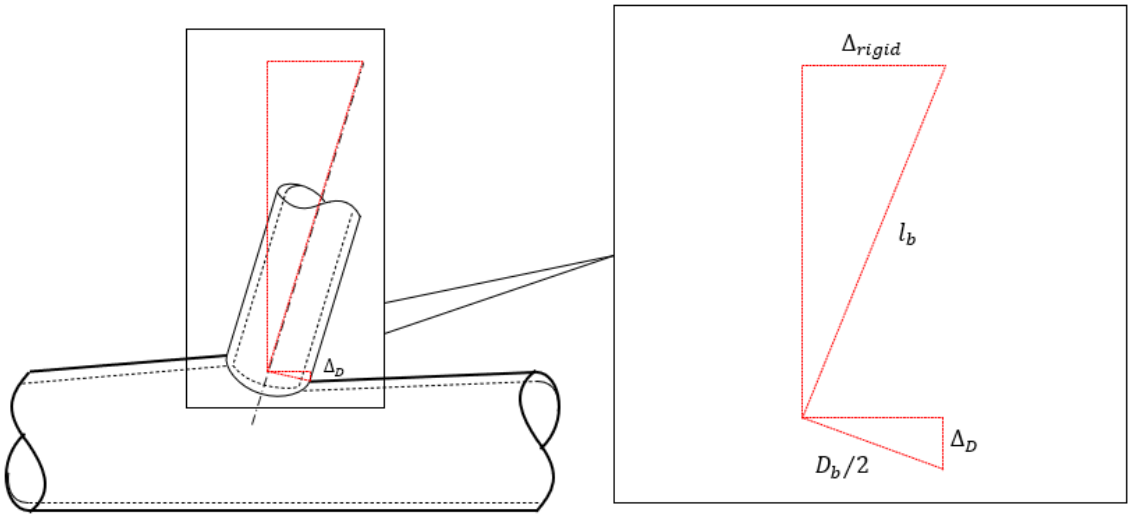

Fig. C.3. Chord indentation calculation geometry

The chord indentation (Δ_D) can be determined as above, by treating the branch in-plane total horizontal deflection (Δ_{total}) as the sum of flexural deflection (Δ_{total}) and rigid body deflection (Δ_{rigid}). This assumption can be deemed accurate when the branch in-plane deflection is very small comparing to the branch length (l_b).

The flexural deflection (Δ_f) can be determined by treating the branch as a cantilever beam:

$$\Delta_f = \frac{P l_b^3}{3 E I_b} \tag{C.1}$$

The total deflection (Δ_{total}) can be obtained in the FE program as the horizontal displacement as the top of the branch. The rigid body deflection (Δ_{rigid}) can be determined as:

$$\Delta_{rigid} = \Delta_{total} - \Delta_f = \Delta_{total} - \frac{P l_b^3}{3 E I_b} \tag{C.2}$$

The chord indentation (Δ_D) then can be determined using the geometry relationship in Fig. C.3:

$$\frac{\Delta_D}{D/2} = \frac{\Delta_{rigid}}{l_b} \quad \text{(C.3a)}$$

$$\Delta_D = \frac{\Delta_{rigid} D_b}{2 l_b} \quad \text{(C.3b)}$$

$$\Delta_{norm} = \Delta_D / D \quad \text{(C.4)}$$

Appendix D: Results of Parametric Study

Test ID	β	2γ	τ	D mm	D_b/t_b	t_w mm	M_{FE} kNm	Δ_{norm} %	$S_{FE\text{-}ip}/S_{n\text{-}ip}$
1	0.4	10	0.20	300	20.00	3.00	30.11	0.19	0.84
2	0.4	10	0.30	300	13.33	4.50	45.20	0.27	0.93
3	0.4	10	0.40	300	10.00	6.00	59.93	0.37	0.98
4	0.4	10	0.50	300	8.00	7.50	74.18	0.47	1.01
5	0.4	10	0.60	300	6.67	9.00	88.48	0.63	1.04
6	0.4	10	0.70	300	5.71	10.50	103.10	0.79	1.07
7	0.4	10	0.80	300	5.00	12.00	117.40	1.00	1.09
8	0.4	10	0.90	300	4.44	13.50	132.67	1.27	1.12
9	0.4	10	1.00	300	4.00	15.00	149.11	1.70	1.15
10	0.4	20	0.30	300	26.67	2.25	22.33	0.20	1.05
11	0.4	20	0.40	300	20.00	3.00	29.81	0.28	1.11
12	0.4	20	0.50	300	16.00	3.75	37.02	0.36	1.14
13	0.4	20	0.60	300	13.33	4.50	43.78	0.47	1.16
14	0.4	20	0.70	300	11.43	5.25	50.55	0.58	1.17
15	0.4	20	0.80	300	10.00	6.00	56.79	0.74	1.17
16	0.4	20	0.90	300	8.89	6.75	63.00	0.94	1.17
17	0.4	20	1.00	300	8.00	7.50	69.02	1.19	1.17
18	0.4	30	0.40	300	30.00	2.00	19.42	0.32	1.15
19	0.4	30	0.50	300	24.00	2.50	23.76	0.43	1.17
20	0.4	30	0.60	300	20.00	3.00	27.81	0.60	1.16
21	0.4	30	0.70	300	17.14	3.50	31.34	0.82	1.15
22	0.4	30	0.80	300	15.00	4.00	34.71	1.19	1.13
23	0.4	30	0.90	300	13.33	4.50	37.97	1.72	1.11
24	0.4	30	1.00	300	12.00	5.00	41.34	2.28	1.10
25	0.4	40	0.60	300	26.67	2.25	19.64	0.81	1.13
26	0.4	40	0.70	300	22.86	2.63	21.81	1.20	1.10
27	0.4	40	0.80	300	20.00	3.00	23.72	1.68	1.06
28	0.4	40	0.90	300	17.78	3.38	25.68	2.30	1.03
29	0.4	40	1.00	300	16.00	3.75	27.98	3.02	1.02
30	0.4	50	0.70	300	28.57	2.10	16.10	1.50	1.04
31	0.4	50	0.80	300	25.00	2.40	17.45	2.06	0.99
32	0.4	50	0.90	300	22.22	2.70	18.89	2.65	0.97
33	0.4	50	1.00	300	20.00	3.00	21.01	3.45	0.98
34	0.4	10	0.20	300	20.00	3.00	34.51	0.35	1.44
35	0.4	10	0.30	300	13.33	4.50	50.47	0.43	1.55
36	0.4	10	0.40	300	10.00	6.00	64.20	0.55	1.57
37	0.4	10	0.50	300	8.00	7.50	76.78	0.60	1.58

Test ID	β	2γ	τ	D mm	D_b/t_b	t_w mm	M_{FE} kNm	Δ_{norm} %	$S_{FE\text{-}ip}/S_{n\text{-}ip}$
38	0.4	10	0.60	300	6.67	9.00	88.52	0.69	1.57
39	0.4	10	0.70	300	5.71	10.50	99.26	0.77	1.55
40	0.4	10	0.80	300	5.00	12.00	108.76	0.88	1.52
41	0.4	10	0.90	300	4.44	13.50	119.99	1.32	1.52
42	0.4	10	1.00	300	4.00	15.00	129.33	1.63	1.50
43	0.4	20	0.30	300	26.67	2.25	25.82	0.36	1.83
44	0.4	20	0.40	300	20.00	3.00	34.01	0.44	1.90
45	0.4	20	0.50	300	16.00	3.75	40.88	0.50	1.89
46	0.4	20	0.60	300	13.33	4.50	46.52	0.68	1.84
47	0.4	20	0.70	300	11.43	5.25	50.88	0.96	1.77
48	0.4	20	0.80	300	10.00	6.00	55.05	1.44	1.70
49	0.4	20	0.90	300	8.89	6.75	60.05	2.14	1.68
50	0.4	20	1.00	300	8.00	7.50	66.05	3.08	1.68
51	0.4	30	0.40	300	30.00	2.00	22.28	0.48	1.99
52	0.4	30	0.50	300	24.00	2.50	26.07	0.66	1.92
53	0.4	30	0.60	300	20.00	3.00	28.45	0.93	1.79
54	0.4	30	0.70	300	17.14	3.50	30.39	1.30	1.67
55	0.4	30	0.80	300	15.00	4.00	32.40	1.79	1.58
56	0.4	30	0.90	300	13.33	4.50	35.08	2.60	1.54
57	0.4	30	1.00	300	12.00	5.00	39.11	3.68	1.56
58	0.4	40	0.60	300	26.67	2.25	19.36	1.14	1.68
59	0.4	40	0.70	300	22.86	2.63	20.42	1.52	1.54
60	0.4	40	0.80	300	20.00	3.00	21.62	2.03	1.45
61	0.4	40	0.90	300	17.78	3.38	23.20	2.73	1.40
62	0.4	40	1.00	300	16.00	3.75	25.86	3.68	1.42
63	0.4	50	0.70	300	28.57	2.10	14.95	1.70	1.44
64	0.4	50	0.80	300	25.00	2.40	15.73	2.22	1.35
65	0.4	50	0.90	300	22.22	2.70	16.94	2.89	1.30
66	0.4	50	1.00	300	20.00	3.00	18.99	3.75	1.32
67	0.55	10	0.20	300	27.50	3.00	64.34	0.32	1.42
68	0.55	10	0.30	300	18.33	4.50	95.09	0.43	1.55
69	0.55	10	0.40	300	13.75	6.00	122.96	0.49	1.59
70	0.55	10	0.50	300	11.00	7.50	147.75	0.49	1.60
71	0.55	10	0.60	300	9.17	9.00	169.67	0.58	1.59
72	0.55	10	0.70	300	7.86	10.50	190.58	0.64	1.57
73	0.55	10	0.80	300	6.88	12.00	208.56	0.73	1.54
74	0.55	10	0.90	300	6.11	13.50	223.00	0.82	1.49
75	0.55	10	1.00	300	5.50	15.00	236.45	1.19	1.45
76	0.55	20	0.40	300	27.50	3.00	63.20	0.44	1.87
77	0.55	20	0.50	300	22.00	3.75	76.38	0.53	1.87
78	0.55	20	0.60	300	18.33	4.50	85.70	0.63	1.80
79	0.55	20	0.70	300	15.71	5.25	92.15	0.79	1.69
80	0.55	20	0.80	300	13.75	6.00	98.10	1.11	1.60

Test ID	β	2γ	τ	D mm	D_b/t_b	t_w mm	M_{FE} kNm	Δ_{norm} %	$S_{FE\text{-}ip}/S_{n\text{-}ip}$
81	0.55	20	0.90	300	12.22	6.75	104.56	1.62	1.54
82	0.55	20	1.00	300	11.00	7.50	111.64	2.35	1.50
83	0.55	30	0.60	300	27.50	3.00	52.49	0.86	1.74
84	0.55	30	0.70	300	23.57	3.50	55.01	1.08	1.60
85	0.55	30	0.80	300	20.63	4.00	57.49	1.38	1.48
86	0.55	30	0.90	300	18.33	4.50	59.84	1.75	1.39
87	0.55	30	1.00	300	16.50	5.00	62.88	2.26	1.33
88	0.55	40	0.80	300	27.50	3.00	38.94	1.54	1.38
89	0.55	40	0.90	300	24.44	3.38	40.24	1.84	1.28
90	0.55	40	1.00	300	22.00	3.75	41.70	2.24	1.21
91	0.55	50	1.00	300	27.50	3.00	30.71	2.28	1.13
92	0.7	10	0.30	300	23.33	4.50	149.43	0.33	1.50
93	0.7	10	0.40	300	17.50	6.00	194.56	0.39	1.56
94	0.7	10	0.50	300	14.00	7.50	237.03	0.41	1.59
95	0.7	10	0.60	300	11.67	9.00	276.47	0.47	1.60
96	0.7	10	0.70	300	10.00	10.50	308.38	0.51	1.57
97	0.7	10	0.80	300	8.75	12.00	333.64	0.61	1.52
98	0.7	10	0.90	300	7.78	13.50	360.55	0.75	1.49
99	0.7	10	1.00	300	7.00	15.00	381.79	0.99	1.44
100	0.7	20	0.50	300	28.00	3.75	120.09	0.46	1.81
101	0.7	20	0.60	300	23.33	4.50	136.51	0.56	1.77
102	0.7	20	0.70	300	20.00	5.25	146.83	0.70	1.66
103	0.7	20	0.80	300	17.50	6.00	153.96	0.89	1.55
104	0.7	20	0.90	300	15.56	6.75	161.02	1.19	1.47
105	0.7	20	1.00	300	14.00	7.50	168.23	1.56	1.40
106	0.7	30	0.70	300	30.00	3.50	88.47	0.99	1.58
107	0.7	30	0.80	300	26.25	4.00	91.54	1.16	1.46
108	0.7	30	0.90	300	23.33	4.50	94.51	1.40	1.35
109	0.7	30	1.00	300	21.00	5.00	98.01	1.69	1.28
110	0.7	40	1.00	300	28.00	3.75	67.26	1.86	1.20
111	0.85	10	0.30	300	28.33	4.50	214.36	0.34	1.46
112	0.85	10	0.40	300	21.25	6.00	276.99	0.29	1.50
113	0.85	10	0.50	300	17.00	7.50	339.95	0.35	1.54
114	0.85	10	0.60	300	14.17	9.00	398.54	0.41	1.56
115	0.85	10	0.70	300	12.14	10.50	451.04	0.47	1.56
116	0.85	10	0.80	300	10.63	12.00	494.52	0.53	1.53
117	0.85	10	0.90	300	9.44	13.50	523.00	0.67	1.46
118	0.85	10	1.00	300	8.50	15.00	557.35	0.90	1.43
119	0.85	20	0.60	300	28.33	4.50	195.60	0.47	1.72
120	0.85	20	0.70	300	24.29	5.25	216.11	0.63	1.66
121	0.85	20	0.80	300	21.25	6.00	226.62	0.77	1.55
122	0.85	20	0.90	300	18.89	6.75	235.46	0.94	1.46
123	0.85	20	1.00	300	17.00	7.50	243.69	1.15	1.37

Test ID	β	2γ	τ	D mm	D_b/t_b	t_w mm	M_{FE} kNm	Δ_{norm} %	$S_{FE\text{-}ip}/S_{n\text{-}ip}$
124	0.85	30	0.90	300	28.33	4.50	142.11	1.29	1.38
125	0.85	30	1.00	300	25.50	5.00	146.09	1.47	1.29
126	1	10	0.40	300	25.00	6.00	377.88	0.25	1.48
127	1	10	0.50	300	20.00	7.50	460.01	0.28	1.51
128	1	10	0.60	300	16.67	9.00	534.84	0.35	1.51
129	1	10	0.70	300	14.29	10.50	614.63	0.40	1.53
130	1	10	0.80	300	12.50	12.00	679.83	0.50	1.52
131	1	10	0.90	300	11.11	13.50	730.93	0.65	1.48
132	1	10	1.00	300	10.00	15.00	769.88	0.81	1.43
133	1	20	0.70	300	28.57	5.25	291.46	0.51	1.62
134	1	20	0.80	300	25.00	6.00	312.75	0.65	1.55
135	1	20	0.90	300	22.22	6.75	327.97	0.79	1.46
136	1	20	1.00	300	20.00	7.50	346.21	1.00	1.41
137	1	30	1.00	300	30.00	5.00	217.95	1.65	1.39